Human Avian Influenza A H5N1, H7N9, H10N8 and H5N6 Virus Infection

3

Pu-Xuan Lu, Yuan Jing, Le Xiao-Hua, Bo-Ping Zhou, Shi Yu-Xin, Zhang Zhi-Yong, Zhou Yu-Shen, Deng Ying-Ying, Ran Xian-Gui, Ge Yang, He Jian, Lin Jia-Fu, Zeng Qing-Si, Li Jing-Jing, Yan De-Min, and Huang Xiang-Rong

3.1 Overview

Yuan Jing

3.1.1 Definition of Human Avian Influenza

Avian influenza is an infectious disease induced by avian influenza viruses in poultry, commonly called genuine fowl plague or European fowl plague.

Human avian influenza is an acute respiratory tract infection caused by some strains of subtypes of avian flu viruses. At present, the subtypes of avian influenza virus confirmed able to infect human beings are H5N1, H7N9, H10N8, H5N6, H7N2, H7N3, H7N7, and H9N2. Among these, human avian influenza H5N1 is severe with a high mortality, which is designated as highly pathogenic avian influenza (HPAI). Since February 2013, 3 cases of human H7N9 avian influenza have been detected in Shanghai City, Anhui province, and Jiangsu province with two dead, which was the first report in the world.

3.1.2 Discovery of Human Avian Influenza

In 1878, a severe disease was firstly reported in Italy among chickens, called fowl plague. In 1901, it was confirmed to be caused by viruses, which were identified as influenza A virus in 1955. In 1981, such disease was formally named avian influenza on the first international avian influenza conference.

3.1.2.1 Discovery of Human Avian Flu Subtype H5N1

On May 5, 1997, H5N1 human avian influenza was firstly found in Hong Kong of China in a 3-year-old child, who died from Reye syndrome and multiple organ failure 10 days after onset of the disease. On May 9, 1997, the US CDC and Rotterdam state influenza center of WHO laboratory isolated the H5N1 AIV strain from the bronchial secretions of this 3-year-old boy, which was named "A/HongKong/157/97." This body is the first case of human infected with highly pathogenic avian influenza H5N1 virus. In December, there were in total 18 cases of human avian influenza confirmed in Hong Kong, China with 6 cases deceased. By December 31, 2014, 667 cases of highly pathogenic human avian influenza H5N1 were documented around the globe, including 393 deaths with the mortality at 58.92 %.

Pu-Xuan Lu (✉)
Department of Radiology, Shenzhen Third People's Hospital Guangdong, Shenzhen, China
e-mail: lupuxuan@126.com

Yuan Jing • Bo-Ping Zhou
Department of Infection, Shenzhen Third People's Hospital Guangdong, Shenzhen, China
e-mail: 13500054798@139.com; zhoubp@hotmail.com

Le Xiao-Hua • Li Jing-Jing • Yan De-Min • Huang Xiang-Rong
The Shenzhen No.3 People's Hospital, Guangdong College, Shenzhen, China

Shi Yu-Xin • Zhang Zhi-Yong
The Shanghai Public Health Clinical Center, Shanghai, China

Zhou Yu-Shen
China's Military Academy of Medical Sciences, Microbial Institute of Epidemic, Guangzhou, China

Deng Ying-Ying
Shenzhen Yantian Hospital, Shenzhen, China

Ran Xian-Gui • Ge Yang
The Second People's Hospital of Fuyang City in Anhui Province, Fuyang, China

He Jian
The First Hospital of Nanchang, Nanchang, China

Lin Jia-Fu
Affiliated Hospital of North Sichuan Medical College, Nanchong, China

Zeng Qing-Si
The First Affiliated Hospital of Guangzhou Medical University, Guangzhou, China

P.-X. Lu, B.-P. Zhou (eds.), *Diagnostic Imaging of Emerging Infectious Diseases*, DOI 10.1007/978-94-017-7363-8_3

3.1.2.2 Discovery of Human Avian Influenza H7N9

Since February 2013, 3 cases were confirmed with avian influenza H7N9 successively in Shanghai, Anhui, and Jiangsu provinces, with 2 cases dead. Besides, this is firstly reported human avian influenza H7N9 in the world. By December 31, 2014, there were in total 451 cases of human avian influenza H7N9 in China, of which 174 cases passed away, with the mortality up to 38.58 %.

3.1.2.3 Discovery of Human Avian Influenza H10N8

On December 6, 2013, 1 case with human avian influenza H10N8 complicated with severe pneumonia was reported in Jiangxi province, China, which was the first around the world. Thereafter, 2 cases of human avian influenza H10N8 were respectively reported on January 25, 2014, and February 13, 2014, in Nanchang Jiangxi province. Of the three cases, 2 cases passed away.

3.1.2.4 Discovery of Human Avian Influenza H5N6

On May 6, 2014, the throat swab of one severe pneumonia case was detected positive for H5N6 avian influenza virus nucleic acid in Sichuan province of China, which was confirmed as avian influenza virus H5N6 via further tests by China CDC. This patient had a history of contact with fowl dead from diseases and was clinically diagnosed with acute severe pneumonia, but passed away due to unresponsive to emergent treatment. This was the global first case. On December 23, 2014, the second human avian influenza H5N6 was found in Guangdong province of China. This male patient was aged 58 years old. Further re-examination by CDC on December 22, 2014, revealed that the avian influenza A H5N6 nucleic acid was positive. This patient is now receiving treatment at the intensive care unit.

3.2 Etiology

Yuan Jing

3.2.1 Morphological Structure and Physiochemical Nature of the Virus

3.2.1.1 Morphological Structure

H5N1 is a segmented negative single-stranded RNA virus belonging to *Influenzavirus A* genus, *Orthomyxoviridae* family of *Mononegavirales* order. The typical shape of avian influenza virus under electric microscope is spherical in a diameter of 80–120 nm and has a capsid in helical symmetry as well as envelope. The initially isolated strains may appear like filament in a diameter of about 20 nm and length of 300–3000 nm. The hemagglutinin protuberance is a homotrimer composed of 3 non-covalently bound protein molecules, and the neural aminase presents with homotetramer made up by head and stem like a mushroom.

The structures of the virus are subsequently envelope, matrix protein, and viral core from inside to outside. The surface glycoprotein club-shaped hemagglutinin (HA) and neural aminase (NA) are embedded into the lipid bilayer of the viral envelope together with ion channel protein. Matrix protein binds to the inner surface of viral envelope and associates with the helical ribonucleoprotein of the viral core to form a layer of membrane-like structure to protect the viral core. RNP comprises nucleocapsid protein (NP), three polymerases (PB1, PB2, PA), and eight viral RNA segments.

3.2.1.2 Physicochemical Properties of the Virus

Similar to human influenza virus, avian influenza virus is sensitive to diethyl ether, chloroform, and acetone and other organic solvents as well as heat and ultraviolet rays. It could be deactivated after exposure to sunlight for 40–48 h and frequently used disinfectants such as sodium hypochlorite, phenolic compounds, quarternary ammonium disinfectants, aquae formalin, and other aldehydes, and iodine compounds could rapidly destroy the infectivity of the viruses. Under general conditions, influenza viruses could survive for 30 days under 0 °C, under 22 °C for 4 days, and under 56 °C for 3 h. Besides, it could be deactivated after half an hour under 60 °C and killed after merely 1 min under over 100 °C. However, under natural conditions, viruses in feces possess tremendous resistance due to protection from organics.

3.2.2 Pathogenicity of the Virus

HA on the envelope of influenza virus, as an attachment protein, could combine with the sialic acid residues of host cell receptors at the top of the globular head, which is key to the viral infection. However, influenza virus could only recognize specific sialic acid molecules on host cell membranes. Neu5Acα2-6Gal binding on the membrane of human respiratory tract mucous cells is key to infection of humans by avian influenza virus. Hyaluronic acid (HA) of the virus combines with host cell receptors and by pinocytosis mediated by such receptors and then enters coated pits which further internalizes HA into coated vesicle. Then the coated vesicle with viruses generates endosome which combines with lysosome to form endosomic lysosome. The acidic pH value inside endosome lysosome changes HA structure and decreases the aggregation force of trimer to expose segment N of HA and fuse with plasma membrane. Besides, the low pH value activates M2 ion channel and facilitates H+ to enter virion, thus decreasing pH value inside the virus. Therefore, the direct interaction between M1 and NP is damaged to free RNP, thus resulting in uncoating of the virus. Thereafter, the genome of the virus is released into the cell plasma and again transported to the nucleus. Both the transcription and repli-

cation of the influenza virus RNA segments take place in the host cell nuclei, and RNP must enter the cell nuclei.

3.3 Epidemiology

Yuan Jing

It has been proved that the avian influenza subtypes able to infect humans are H5N1, H7N9, H10N8, H5N6, H9N2, H7N7, H7N2, and H7N3, of which H5N1 presents with relatively strong infectiveness and causes severe conditions and high mortality. Besides, in 2013, patients infected with H7N9 avian influenza also manifested relatively severe conditions and high mortality.

3.3.1 Sources of Infection

Avian influenza viruses have been confirmed widely distributed in many poultry (including the turkeys, chicken, guinea fowl, pigeons, geese, and ducks) and wild fowl (including wild ducks, swans, and various kinds of sea birds) with diseases induced by avian influenza viruses in domesticated chicken and turkey most severe. Besides, there exists silent infection in domesticated poultry which could prolong several months.

The poultry infected by avian influenza or carrying avian influenza virus such as chicken, ducks, geese, and pigeons, particularly chicken, serve to be the important source of infection. The secretions and excretions, feathers, tissue organs, and fowl eggs may also carry viruses.

The influenza A virus could also be seen in humans, horses, pigs, monkeys, domestic cats, rats, tigers, and American leopards, and occasionally in ferret-polecat, seal, whales, and other mammals. In 1970, Kundin found H3N2 subtype antibodies in pigs and isolated similar virus.

Whether human could spread infection needs to be further consolidated, and whether patients with human avian influenza are source of infection has not been determined. Besides, human avian influenza H5N1 and H7N9 are also reported in individual interpersonal infection case.

3.3.2 Route of Transmission

Avian influenza viruses is mainly disseminated through the feces and excretions of infected poultry, contaminated drinks, drinking water, egg holders, chicken embryos, gas-soluble gels, poultry eggs, transportation tools, and other channels. This virus could spread the infection through human respiratory tract, digestive tract, gas-soluble gel, as well as skin damages and eye conjunctiva, particularly respiratory tract and digestive tract. Direct contact with infected poultry or indirect contact with viral pollutants is also regarded as the main route of infection; viral secretions, feces, and any subjects contaminated by poultry corpses could also transmit the epidemic; direct contact with the viral strains could also spread this disease.

3.3.3 Susceptible Population

Considering human avian influenza cases already detected, patients of any case could be infected irrespective of gender.

3.3.4 Epidemiological Characteristics

3.3.4.1 Season of Epidemic

There could be epidemic in all the four seasons, but mainly in the alternate season between winter and spring as well as between autumn and winter, so frequently upon sudden attack of cold current and drastic change of temperature. Generally, human avian influenza is seldom reported in summer but could also occur sporadically such as the first case of avian influenza H5N1 in Shenzhen of China in June. The newly emerging human avian influenza H7N9 in 2013 in China also mainly occurred in February to March.

3.3.4.2 Area Distribution Characteristics of Avian Influenza

Human avian influenza develops mainly in the vast village areas in various countries in the world. In China, the highly pathogenic human avian influenza epidemic is mostly documented in rural areas and surrounding areas of provincial capitals. Meanwhile intimate contact with dead poultry and their secretions and excretions provide main conduit for dissemination of human avian influenza.

3.3.4.3 Human Population Distribution Characteristics

Among patients with human avian influenza, children and the young people occupy a relatively high proportion, and the ratio between the male and female is at 7: 14, with the latter remarkably higher than the before. Besides, farmers and rural students or children take a large proportion. However, for avian influenza H7N9, the middle old-aged account for a relatively high proportion.

3.4 Pathogenesis and Pathological Changes

3.4.1 Pathogenesis

Influenza virus belongs to influenza virus genus of orthomyxovirus family and is an enveloped, negative single-branded and segmented RNA virus. Influenza virus falls into type A, type B, and type C in light of the antigen of nucleoprotein (NP). Influenza virus type A could be further divided

into subtypes according to the antigen difference of hemagglutinin (HA) and neuraminidase (NA) embedded in the lipid bilayer outer membrane. Avian influenza virus (AIV) of different types or subtypes demonstrates varying pathogenicity due to the difference in viral genome structure and sequence expressing protein polypeptide. Some mutant viruses could even surmount genus and order barriers to infect humans, such as H5N1, H7N7, H9N2, and H7N9, among which H5N1 or H7N9 infection could induce severe conditions and high mortality.

HA on the outer membrane of influenza virus type A plays critical roles in the pathogenesis of AIV. HA, as the main component of envelope spike, is key to viral attachment and transmembrane process and could stimulate generation of neutralizing antibody and cellular immunity to ward off viral infection and disease. In the course of infection, HA, could be hydrolyzed into peptide chain HA1 and HA2, with the former able to combine with host cell receptors and the latter as a critical subunit to mediate fusion of the virus and host cell membranes. Therefore, the influenza virus could integrate with host cell receptors mediated by HA1 and fuse with cell membrane mediated by HA2 to promote release of ribonucleoprotein (RNP).

Another important component of highly pathogenic AIV infecting human body cells may be NS1 protein, which could inhibit interferon (IFN) and tumor necrosis factor-alpha (TNF-α). Fas signal pathway may mediate cell apoptosis related to influenza virus infections. The inflammatory reaction factors may mediate the systematic inflammatory reaction syndrome in severe patients, acute respiratory distress syndrome, and multiple organ failure, while corticosteroids may delay or decrease such reactions, suggesting that immune injury may participate in pathogenesis of human avian influenza.

3.4.2 Pathological Changes

Highly pathogenic human avian influenza is induced by human avian influenza virus H5N1 and H7N9 characteristic of acute respiratory system lesions and with high mortality. In light of domestic and foreign literature reports, its main pathological changes could be summarized as severe lung disease, toxic changes, and secondary infections of immune organs and other viscera. Main causes of death include (1) progressive respiratory failure incurred by pulmonary diffusive alveolar injury; (2) complication with multi-organ damages such as liver, kidneys, and heart; and (3) immunosuppression and secondary infections.

3.4.2.1 Lungs

Naked-Eye Observation

Lung tissues are revealed swollen and heavier, with the left lung up to 770–2250 g and right lung 785–800 g (both lungs 1550–1950 g). Both lungs present with dark red color and distinct consolidation, particularly at the lower lobes of the lungs. There may be slight adhesions between the lungs and parietal pleura. Lung sections demonstrate notable congestion and edema as well as exudation of light red bubbly blood-stained fluids. Trachea and bronchi are viewed with congestion at mucosa and light red bubbly secretions inside the lumen. The pleural cavity is observed with slight light yellow effusions.

Examination Under Light Microscope

Early phase: It manifests diffuse alveolar injury at both lungs, typical of acute disseminated exudative disease. The alveolar spaces are full of pinkish exudates and inflammatory cells of varying amount, including mainly lymphocytes, monocytes, plasma cells, and macrophages as well as a few neutrophilic granulocytes. The alveolar spaces could also be seen with exfoliated, degenerated, and necrotic alveolar epithelial cells. Part of the alveolar spaces are found with bleeding and fibrin as well as hyaloid membrane. Alveolar type II epithelial proliferation is also observable. No inclusion bodies are observed in megakaryocytes and nucleus or plasma. Part of the alveolar septum become lightly thicker with vascular dilatation, congestion, and inflammatory cell (type similar to that inside alveolar space) infiltration but without intravascular fibrinous thrombi. Middle phase (disease course over 10 days): it presents changes of proliferation phase. Diffuse alveolar damages and alveolar epithelial reactive proliferation are seen but cellular changes related to virus absent. Alveolar space is seen with fibrinous exudation, bleeding, formation, and mechanization of hyaloid membrane. Interstitium is detected with vascular congestion, reactive fibroblast proliferation, and light lymphocyte infiltration. Part lung tissues are found with fungal infections. Advanced phase (disease course over 3 weeks): it presents changes of fibrosis. Part alveolar epithelium is revealed with necrosis and exfoliation as well as reactive proliferation (Figs. 3.1 and 3.2) but without viral inclusion body in epithelial cells. Alveolar spaces are observed with effusion of plasma fluid, fibrin, red cells, and neutrophilic granulocytes, formation of hyaloid membrane, organization of squamous epithelia, and mechanization of exudates (Fig. 3.3). Part alveoli are detected with collapse or compensatory emphysema. Pulmonary interstitium is seen with fibrosis and occasional presence of lymphocytes, plasma cells, and reactive hemophagocytes. Pulmonary interstitial capillaries are viewed with transparent emboli and DIC as well as occasionally obliteration (Fig. 3.4). Pulmonary bleeding and secondary infection could also be seen.

3.4.2.2 Immune Organs

Lymph Nodes

Lymphocytes decrease and scatters and lymph sinus is found dilated and with focal necrosis. Histiocytes proliferate

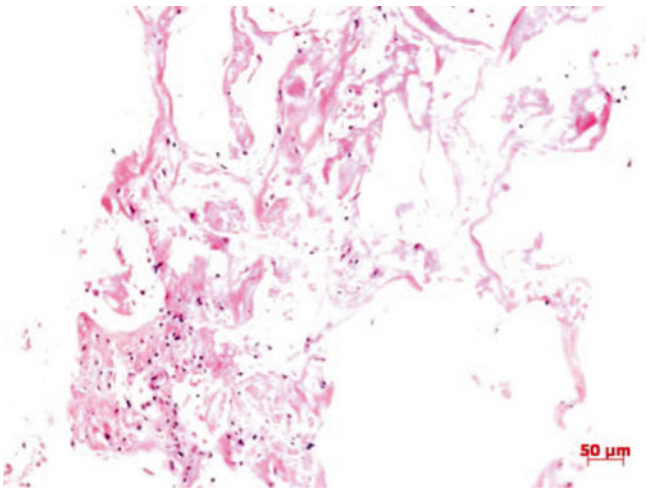

Fig. 3.1 Degeneration and necrosis of lung tissues and light lymphocyte infiltration HE staining

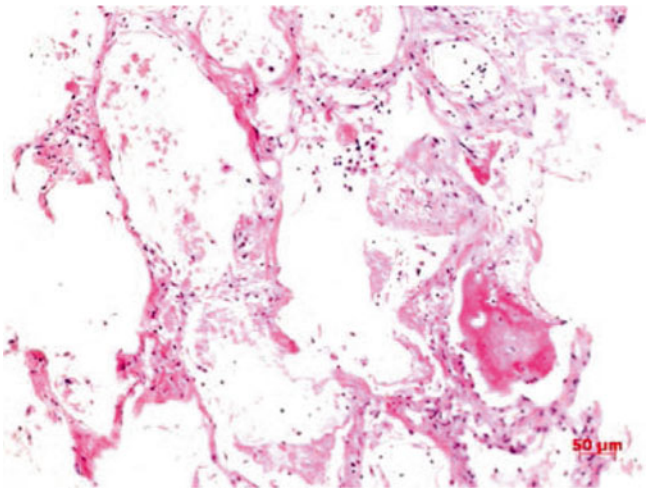

Fig. 3.3 Exfoliation of alveolar epithelia, and presence of reddish liquid, fibrin and slight amount of lymphocytes in pulmonary alveolar spaces. HE staining

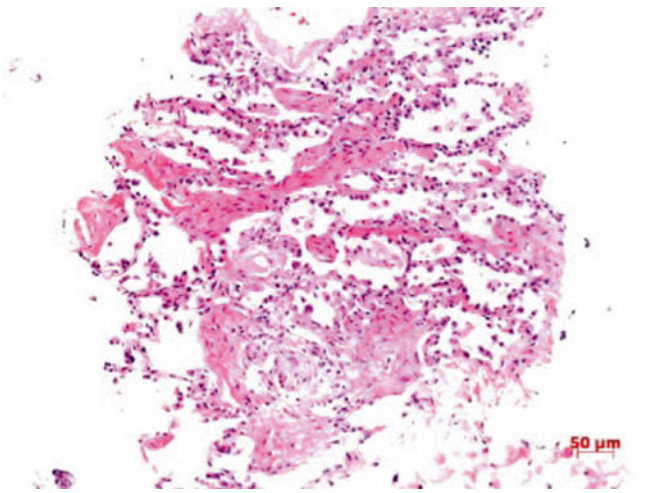

Fig. 3.2 Reactive proliferation of alveolar epithelium and fibrosis of pulmonary interstitium HE staining

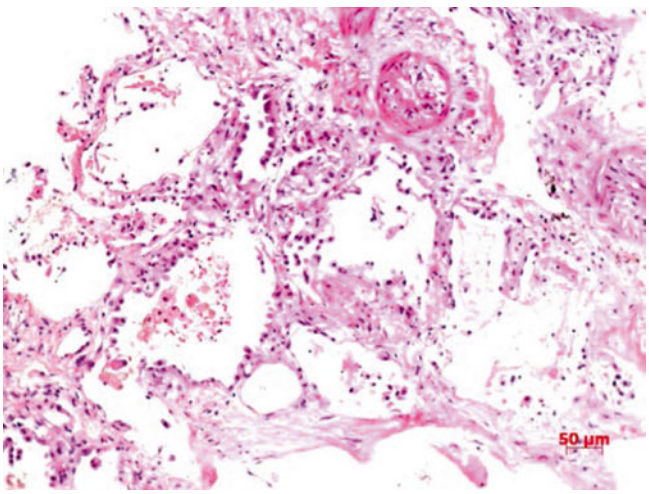

Fig. 3.4 Proliferation of lung epithelial cells, with partial exfoliations, and vascular occlusion HE staining

accompanied by phenomenon of phagocytosis of the hemophagocytes and lymphocytes.

Spleen

The spleen presents with mild enlargement, smooth surface, and dark red color. Microscopy suggests extravasated blood, edema, atrophy of white marrow, and enlargement of red marrow. Peripheral to the white marrow is atypical lymphocytes. Part spleen sinuses are seen with slight inflammatory cell infiltration and histiocytosis accompanied by hemophagocytosis.

Bone Marrow

Bone marrow tissues are revealed with reactive histiocytosis and hemophagocytosis.

3.4.2.3 Other Main Organs

Cerebrum, Cerebellum, and Spinal Cord

The brain is unveiled with extravasated blood at the surface blood vessels and slight widening of gyrus. Microscopy visualizes wider spaces between the cerebrum, cerebellum, and spinal nerve cells and small blood vessels, as well as extravagated blood in blood vessels.

Heart

Cardiac chambers are found with dark-brown blood clots. Microscopy indicates degeneration of cardiocyte vacuole and cardiocytes with swelling and loss of striated patterns as well as partial pyknosis. Interstitium manifests light edema and extravagated blood in blood vessels.

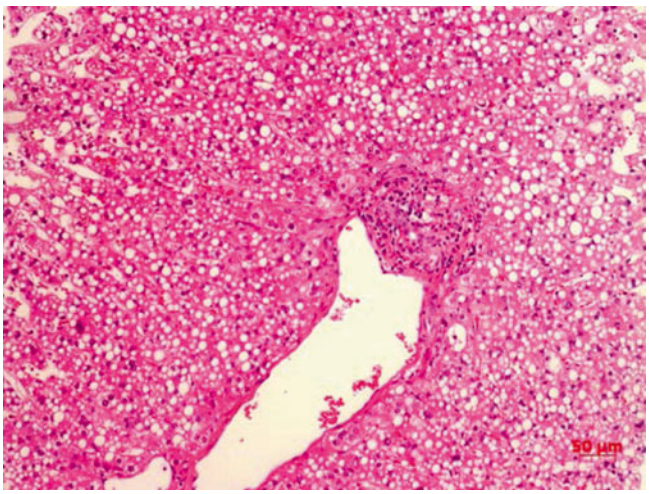

Fig. 3.5 Presence of lipid droplets at liver cellular plasma and slight lymphocyte infiltration at the portal area HE staining

Liver

The surface of the liver is smooth, grayish red, and with homogeneous section. The liver lobule presents normal structure, with slight hydropic degeneration and fat degeneration (Fig. 3.5) at liver cells and central necrosis. Interstitium is unveiled with light extravagated blood and part portal area with light lymphocyte infiltration.

Kidney

The kidney becomes swollen and the renal capsule is easily to be separated. The cortex and medulla are well demarcated with slight blood stasis at the latter. Under the microscope, multiple glomerular capillaries are seen with dilatation and blood stasis, and the renal tubules with necrosis. The blood vessels of renal interstitium are revealed with extravagated blood and thrombosis.

3.5 Laboratory Examination

Yuan Jing

3.5.1 Blood Routine Examination

Patients with human avian influenza are characterized by decrease of the peripheral blood WBC count, particularly decrease of lymphocytes, which meanwhile is closely related with the occurrence of ARDS and mortality rate.

3.5.2 Blood Biochemical Examination

Creatine kinase, lactate dehydrogenase, aspartate aminotransferase, and alanine aminotransferase are mostly found elevated and so are C-reactive protein and myoglobin.

3.5.3 Virus Antibody and Virus Nucleic Acid Test

3.5.3.1 Immunofluorescence Test

Influenza viruses infect mainly the epithelial cells of respiratory tract. Positive experiment suggests that this patient or cultured subject has influenza virus and could directly conclude infection of the corresponding type or subtype of influenza virus. This experiment is superior in specificity and sensitivity, which are 5–10 times higher than direct immunofluorescence assay.

3.5.3.2 Colloidal Gold Test

The sample extract from the test kit is mixed with any clinical specimen to separate virus antigens, which are then dropped on the test membrane already adsorbed with alkaline phosphatase-labeled anti-influenza virus A nucleoprotein monoclonal antibody and substrate liquid. The thorough reaction between the antigen and antibody could develop color under the catalysis of enzymes.

This method is applicable to quantitative measurement of influenza virus A and B in nasal suction liquid, nasal scrubbing liquid, and laryngopharyngeal scrubbing liquid specimens.

3.5.3.3 Enzyme-Linked Immunosorbent Assay (ELISA)

Competitive block method is adopted to test H5 antibodies in the serum specimen. The coating monoclonal antibodies on the microwell plate of the agent kit are added with serum specimen and antigen reaction liquid, which forms "coating monoclonal antibody-antigen specimen antibody" complex. Then enzyme-marked antibodies are added. If the serum specimen could distinctly inhibit the combination of enzyme-marked antibodies with antigens, it suggests the presence of avian influenza H5 antibodies.

1. Cutoff value: The Cutoff value = average negative control OD × 0.5
2. Positive judgment: Sample OD value <Cutoff value indicates positive, and otherwise negative. Rise of serum H5 antibodies by four or above times in the early stage of onset and stage of recovery could serve as evidence for definitive diagnosis.

3.5.3.4 Nucleic Acid Test

Polymerase chain reaction (PCR), as a molecular biological assay, could test avian influenza virus nucleic acid in various specimens (blood, feces and excretion, respiratory secretions, and tissue secretions).

3.5.3.5 Virus Isolation

Chicken-embryo culture is a common method of viral culture which is simple to operate and easy to manage. It is very sensitive to orthomyxovirus, paramyxovirus, Poxvirus, and herpes

virus and could be used to separate afore viruses from patient samples. The frequently used method for influenza virus is double chicken embryo allantoic cavity and amniotic cavity inoculation. If the chicken embryo dies after 24 h or HA test is positive, it indicates presence of viral infection and CF, IF, EIA, HI, and NT shall be conducted further for differentiation.

In case of diagnosis of suspected cases, both the titer of serum-neutralizing antibody in the acute and recovery periods shall be tested, which could establish diagnosis if the serum antibody level in latter is higher than that the former (≥4). In children, particularly those below 3 years old, the titer of serum influenza virus antibody increasing by two times holds diagnostic value.

3.6 Clinical Diagnosis

Yuan Jing

3.6.1 Diagnostic Criteria

The diagnosis of human avian influenza could be derived based on epidemiological history, clinical manifestation, and laboratory examination results. If the epidemiological history is not clear, diagnosis of human avian influenza H5N1, H7N9, H10N8, and H5N6 could be reached according to clinical manifestations, supplementary examinations, and laboratory test results, particularly separation of avian influenza H5N1, H7N9, H10N8, and H5N6 from patient respiratory tract secretions; avian influenza virus H5N1, H7N9, H10N8, and H5N6 nucleic acid test positive; or avian influenza virus H5N1, H7N9, H10N8, and H5N6 specific antibody level in double serum samples 4 times or above higher by dynamic test.

3.6.2 Severe Human Influenza Diagnostic Criteria

The presence of any of the following five items could conclude diagnosis of severe human avian influenza:

1. Dyspnea: The adult respiratory rate under resting state is ≥30 times/min concurrently with either following circumstance: (i) chest imaging suggests that multilobar lesions or foci occupy over 1/3 of the total area of both lungs on orthotopic film and (ii) conditions progress with lesions increasing by over 50 % and accounting for over 1/4 of total area of both lungs on orthotopic film within 40 h.
2. Distinct hypoxemia: Oxygen inhalation at 3–5 L/min, arterial partial pressure of oxygen (PaO2) <70 mmHg (1 mmHg = 0.133 kPa), or pulse blood oxygen saturation (SpO2) <93 %, or already diagnosed as acute lung injury (ALI) or acute respiratory distress syndrome (ARDS). If the oxygenation index is below 300 mmHg (1 mmHg = 0.133 kPa), it could be diagnosed as ALI; and if the oxygenation index is below 200 mmHg, it could be diagnosed as ARDS.
3. Occurrence of shock or multiple organ dysfunction syndrome (MODS).
4. Occurrence of viral encephalitis.
5. Infected children manifest Reye syndrome.

3.7 Chest Imaging Diagnosis

For imaging examination of human avian influenza virus pneumonia, CT possesses distinct advantages, which could contribute to accurate determination of the degree, extent, and site of lung injury and identify the meticulous dynamic changes of lesions via the high resolution of tissue density and adjustment of window breath and position to obtain more information about lesions than chest X-ray, therefore offering evidence for clinical diagnosis and treatment. Lung interstitial fibrosis is an important complication of this disease, and high-recognition CT (HRCT) can better visualize the subtle changes of pulmonary interstitial fibrosis, such as pulmonary lobular septum thickening, and subpleural curvature shadow, which could aid efficacy evaluation and prognosis estimation.

3.7.1 Chest Manifestations of Human Avian Influenza Virus Pneumonia

3.7.1.1 Early Phase of Onset

The incubation phase of patients with human avian influenza H5N1, H7N9, H10N8, and H5N6 is commonly 1–7 days, mostly 2–4 days, but may last 8 days in a few patients. After the incubation ensues, the early phase of the onset which generally prolongs 1–4 days. The initial symptom is fever with body temperature >38°C, and over half of the patients are accompanied with influenza-like symptoms such as chilliness, headache, soreness of joints and muscles, fatigue, dry and nonproductive cough, as well as chest pain. Chest X-ray or CT inspections may be manifested as (1) lobular septum thickening and acinar nodular shadows; (2) solitary or multiple patchy ground-glass shadows in the lungs and lesions mostly located at unilateral inferior lung lobe; and (3) patchy pulmonary consolidation shadows with air bronchogram in between or ground-glass shadows at the periphery or other long lobes (Figs. 3.3, 3.4, 3.5, and 3.6).

3.7.1.2 Progression Phase

The lesions aggravate within 14 days after the onset in most patients. The patchy shadows of the early phase progress into large patchy, multiple, or diffusive lesions in 3–7 days. The lesions may extend from unilateral to bilateral lungs and from single lung lobe to multiple lobes. In progression phase, severe patients manifest multilobar lesions or lesions advancing by over 50 % within 48 h (Fig. 3.7).

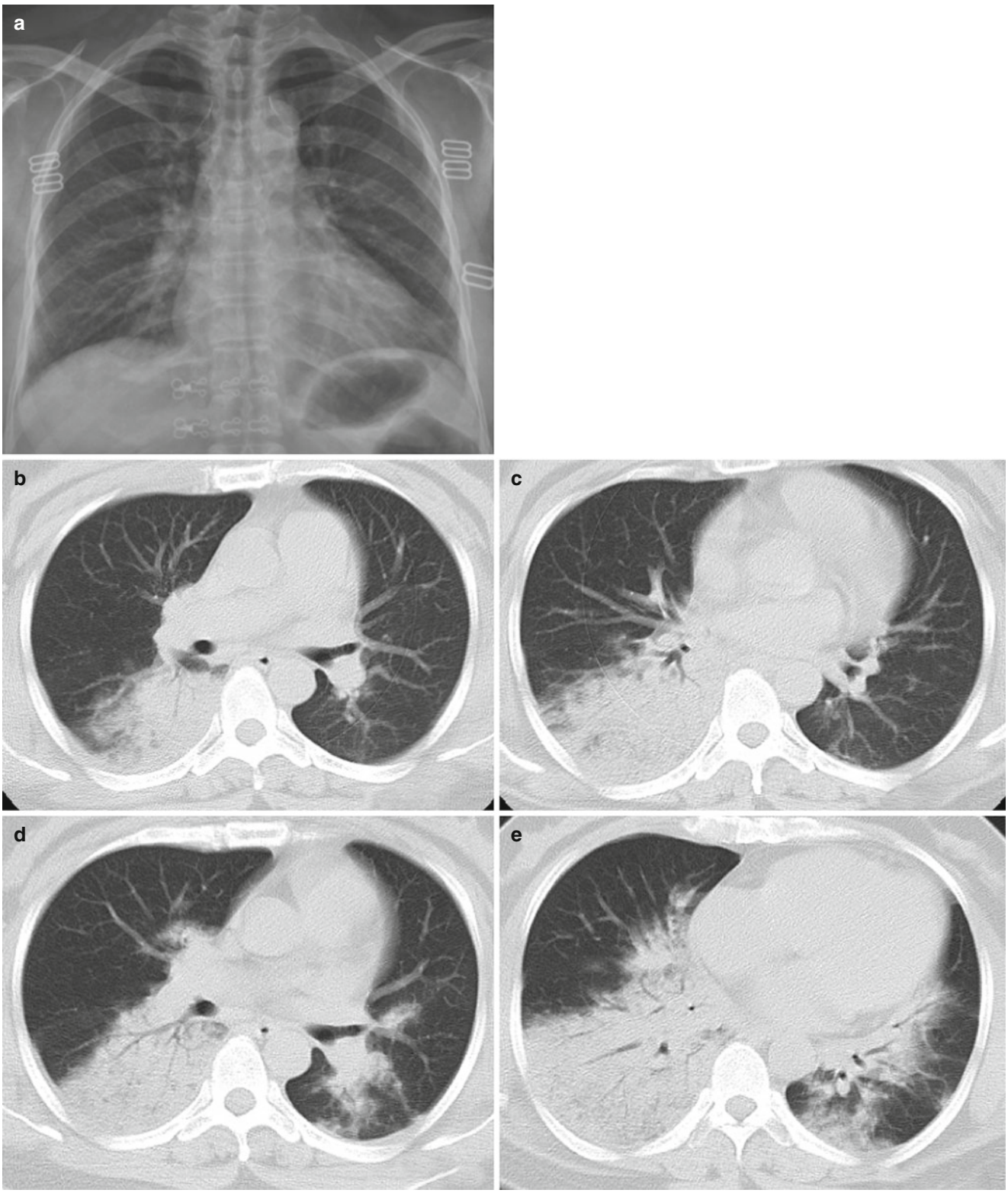

Fig. 3.6 (**a**–**e**) The female patient aged 39 years old is infected with avian influenza virus H7N9 pneumonia. (**a**) On 2nd day after onset, chest X-ray plain films of both lungs did not detect distinct abnormalities. (**b**, **c**) On 4th day after onset, chest CT scan visualized large patchy consolidation shadow at posterior basal segment of right lung inferior lobe, with air bronchogram in between. (**d**, **e**) On 6th day after onset, chest CT scanning revealed that the large patchy consolidation shadow at the right lung inferior lobe progressed notably and the basal segments of right lung middle lobe and left lung inferior lobe were observed with scattering plaque or large patchy consolidation shadows and ground-glass shadows at the periphery

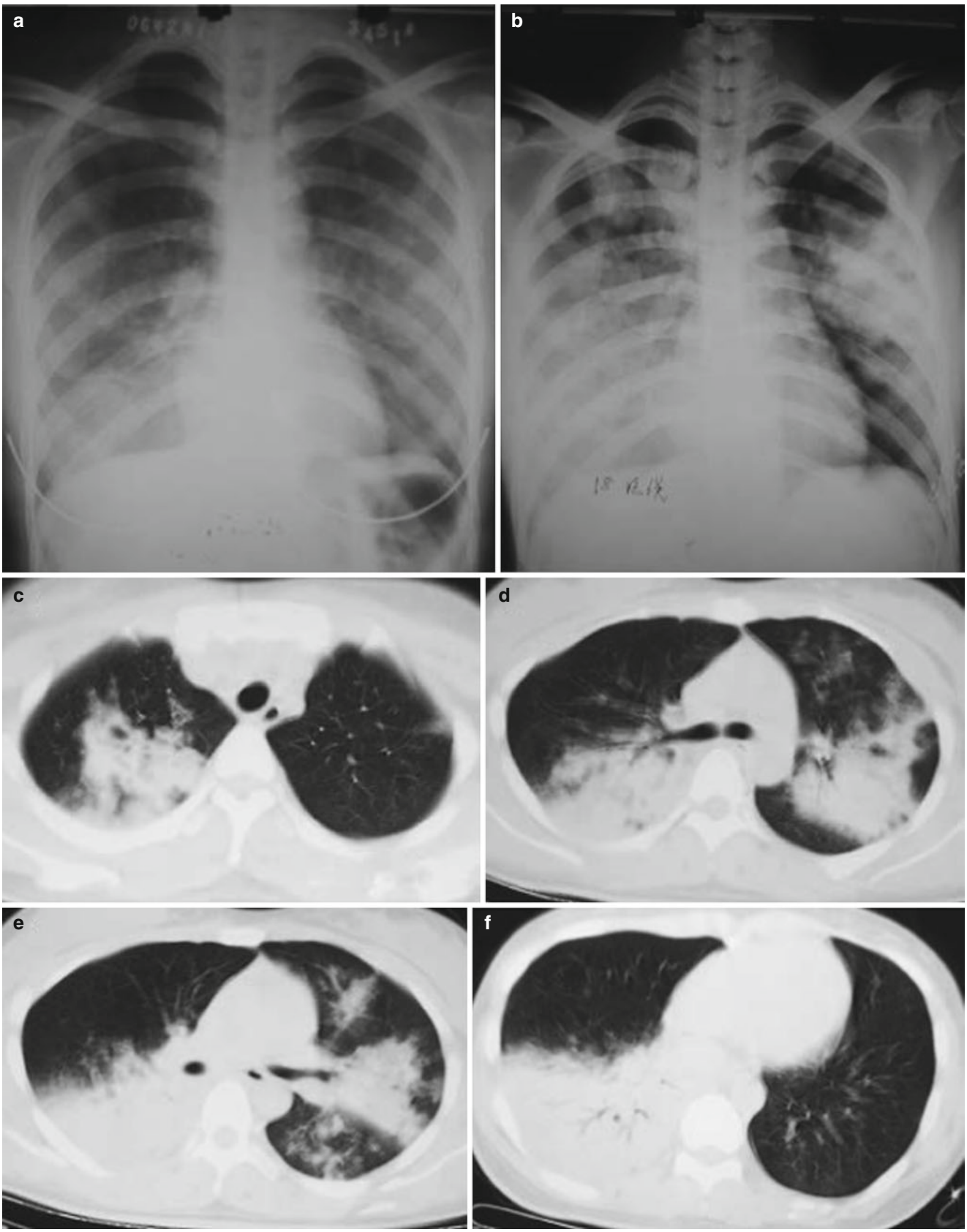

Fig. 3.7 (**a**–**f**) The female patient aged 26 years old was infected with avian influenza H5N1. (**a**) On the 6th day of the onset of the disease. Chest X-ray revealed large patchy ground-glass shadows at both middle and inferior lung fields and consolidation shadows at the right inferior lung. (**b**) On the 7th day of the onset of the disease. Chest X-ray unveiled rapid development of lesions, with the foci at both lungs enlarging distinctly. Extensive consolidation shadows were seen in both lung fields. (**c**–**f**) On the 7th day after onset of the disease. The CT lung window showed: The middle and inferior right lung lobe manifested large patchy consolidation shadows, with air bronchogram inside. The left lung was visualized with large patchy consolidation shadows and patchy ground-glass shadows

Chest Imaging Presentations

1. Most frequently seen is large patchy consolidation shadows at the lungs, with air bronchogram inside; plaque-shaped consolidation shadows could also be seen, with foci distributed at lung lobes or lung segments or quasi-circular consolidation shadows of varying sizes observable (Figs. 3.3, 3.4, 3.5, 3.6, 3.7, and 3.8).
2. Lung consolidation shadows and ground-glass dense shadows appear concurrently, predominantly consolidation (Figs. 3.3, 3.4, 3.5, 3.6, 3.7, 3.8, and 3.9).
3. In severe cases, both lungs develop disseminated infiltration foci and ground-glass shadows observable at the anterolateral large patchy lung consolidation shadows, presenting ARDS changes (Figs. 3.3, 3.4, 3.5, 3.6, 3.7, 3.8, 3.9, and 3.10).

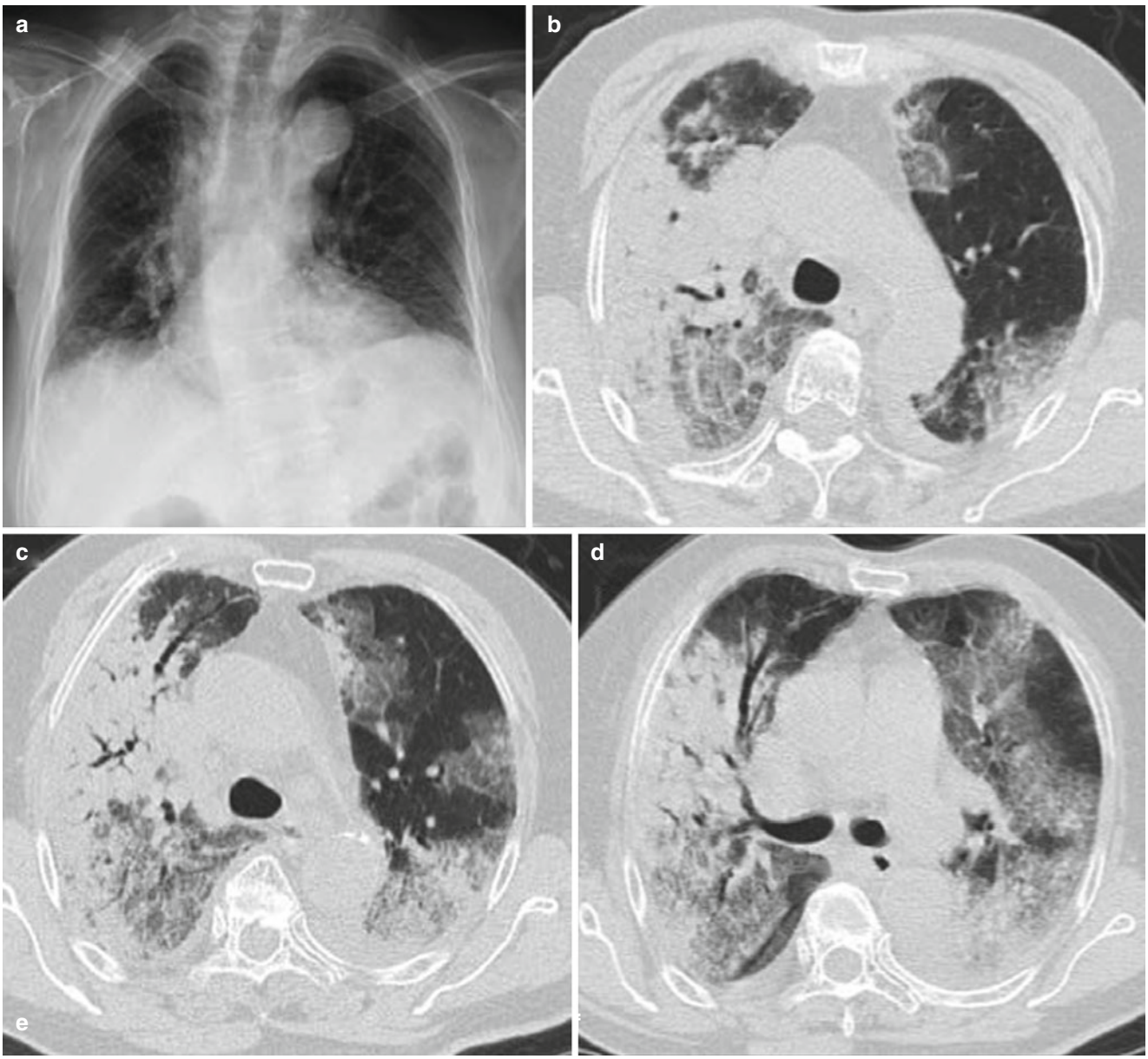

Fig. 3.8 (**a**–**e**) The female patient aged 82 years old was infected with avian influenza H7N9 pneumonia. (**a**) On the 4th day of the onset of the disease, chest X-ray visualized thickening of lung textures at both inferior lungs, but no distinct consolidation shadows inside the lungs. (**b**–**e**) On the 6th day of the onset of the disease, chest CT lung window viewed extensive ground-glass shadows and consolidation shadows at both lungs, with mainly consolidation shadows at the right lung lobes and air bronchogram observable. The left inferior lung was found with consolidation and left superior lung with mainly ground-glass shadows. (**f**) On the 6th day of the onset of the disease, chest CT longitudinal window indicated consolidation shadows at both lungs accompanied by slight effusions in the right thoracic cavity

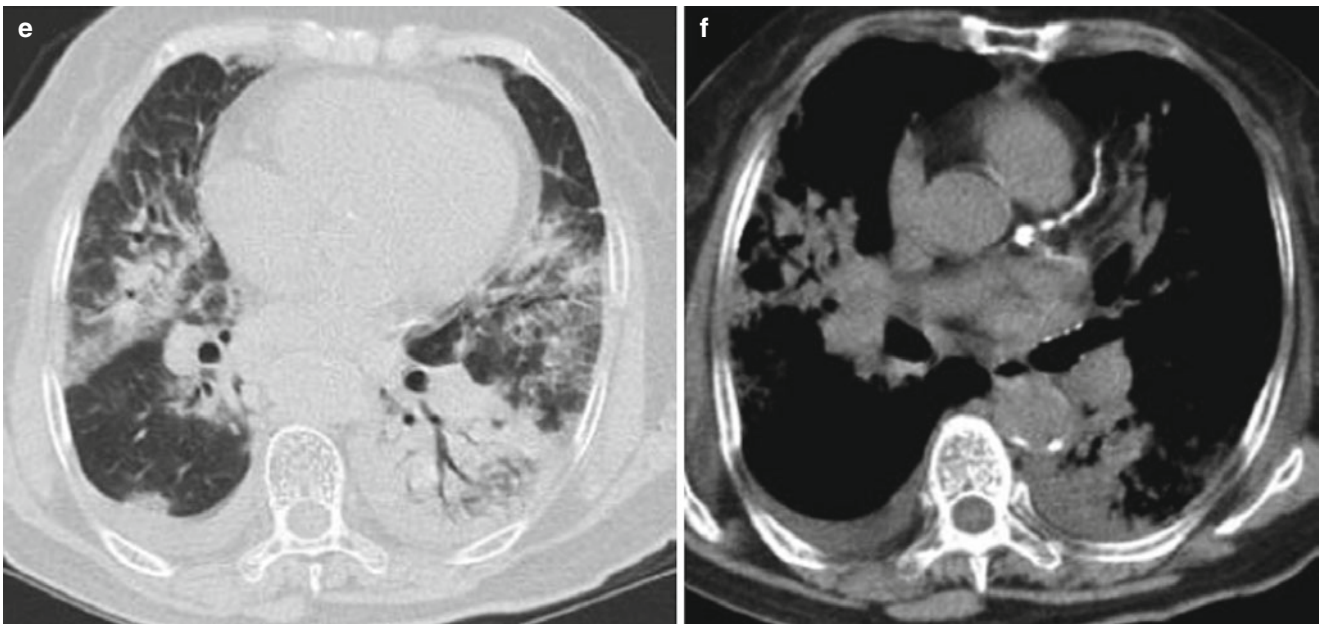

Fig. 3.8 (continued)

4. Pleural effusion is relatively common, particularly in patients with severe pneumonia. The absorption of pleural effusion and lung foci are synchronous generally.

3.7.1.3 Phase of Recovery

After effective treatment in progression phase, the conditions of patients with human avian influenza pneumonia are under control and foci begin to be absorbed. The majority foci of patients with human avian influenza virus pneumonia free of secondary infections are completely absorbed within 30 days, while the lungs of part of the patients may present with fibrosis or proliferation of lung interstitium. For a few severe patients, the foci absorption is relatively slow, and absorption of lung shadows still takes a relatively long time, even years, resulting in interstitial fibrosis. Imaging presentations in the phase of recovery: (1) The large patchy pulmonary consolidation shadows are gradually absorbed and become smaller and light in color, and the consolidation pulmonary tissues gradually swell. Imaging presentations are characterized by plaque-shaped and striped consolidation shadows. (2) Ground-glass-density shadows shrink gradually or are completely absorbed. (3) Pulmonary interstitium presents with fibrosis typical of lobular septum thickening, subpleural curvature shadows, paraseptal emphysema, paramediastinal pulmonary bulla, and bronchiolar dilation (Figs. 3.3, 3.4, 3.5, 3.6, 3.7, 3.8, 3.9, 3.10, and 3.11). (4) The pleura shows limited thickening and adhesion. (5) Pulmonary air sacs are observable during absorption of lesions, which might be induced by pulmonary parenchymal necrosis and formation of valves and could be absorbed after treatment (Figs. 3.3, 3.4, 3.5, 3.6, 3.7, 3.8, 3.9, 3.10, 3.11, and 3.12).

3.7.1.4 Characteristics of the Dynamic Changes of Human Avian Influenza Virus Pneumonia

The characteristic dynamic changes of human avian influenza virus pneumonia are as follows: ① The foci present with rapid dynamic changes, and the foci in severe pneumonia cases could disseminate to multiple lobes and segments within 48 h. ② Lesions in the early phase and progression phase mainly manifest as consolidation shadows and ground-glass shadows. ③ Absorption of the foci is slow. Some patients may present with lung interstitial fibrosis in the lungs several years after discharge (Figs. 3.3, 3.4, 3.5, 3.6, 3.7, 3.8, 3.9, 3.10, 3.11, 3.12, and 3.13). ④ During the course of absorption in recovery phase, the foci in the middle and upper lung lobe are absorbed at an earlier time than those in the dorsal inferior lung lobes and subpleura; and foci firstly formed in the early and progression phase are absorbed at a later time. On the contrary, foci that appear at a later time are absorbed more early. ⑤ Chest imaging changes and clinical symptoms and signs are inconsistent, that is a delay of imaging signs of absorption of pulmonary lesions from clinics (Figs. 3.3, 3.4, 3.5, 3.6, 3.7, 3.8, 3.9, 3.10, 3.11, 3.12, 3.13, and 3.14).

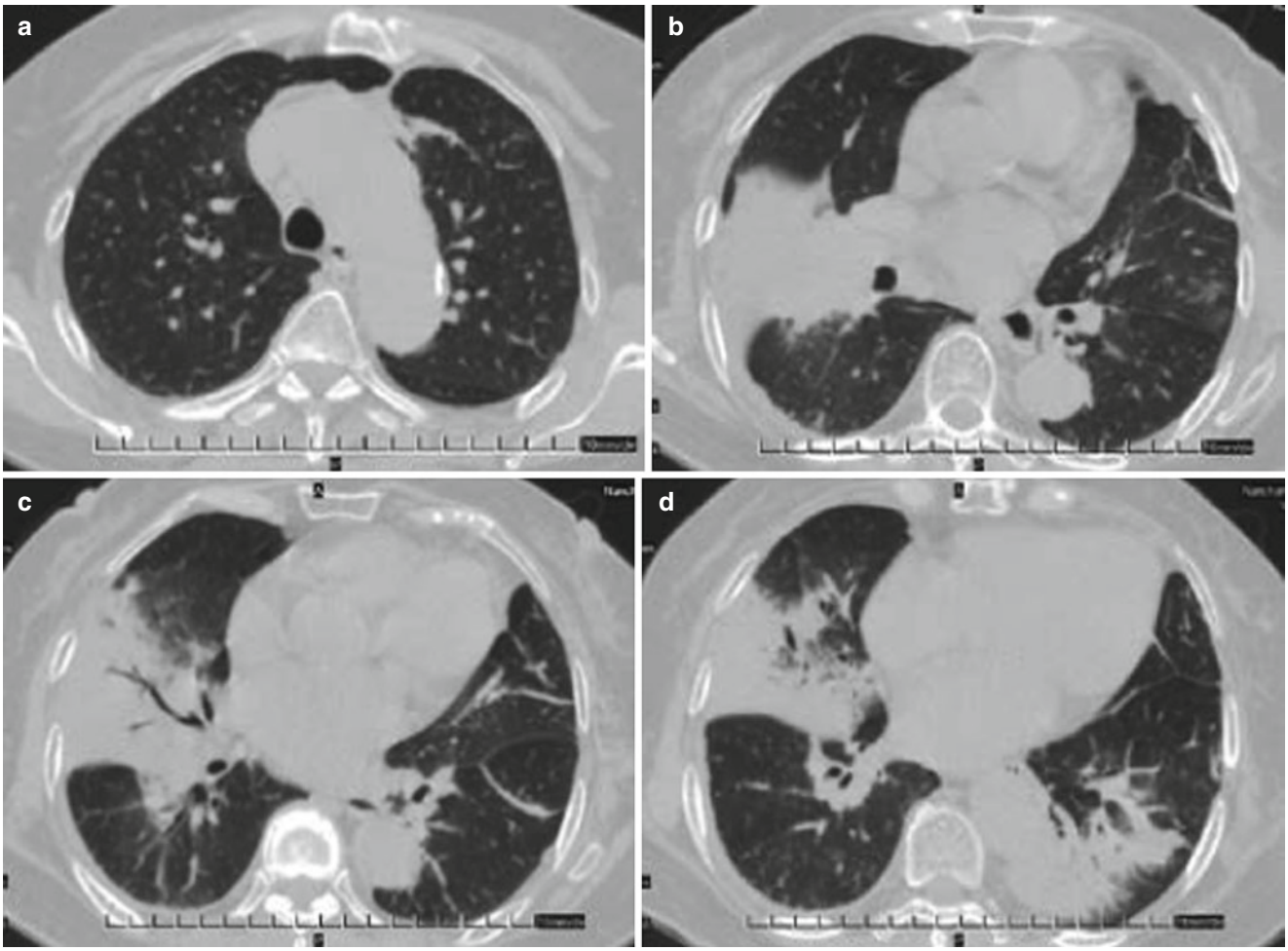

Fig. 3.9 (**a**–**d**) The female patient aged 73 years old was diagnosed with avian influenza H10N8 pneumonia and underwent chest CT on December 1, 2013 (on the 4th day of onset of the disease). (**a**) Beside the left superior lung aortic arc, patchy shadows of increased density were observed. (**b**) Right middle lung lobe was seen with large patchy consolidation shadows and left superior lung with patchy ground-glass-density shadows. (**c**) Right middle lung lobe was found with large patchy consolidation shadows, with air bronchogram in between, and left inferior lung with cord-shaped high-dense shadows. (**d**) Large patchy consolidation shadows were detected beside the right middle lung lobe and left lung lobe thoracic aortic arc

3.7.2 Imaging Differential Diagnosis of Human Avian Influenza Pneumonia

The imaging manifestations of human avian influenza pneumonia comprise disseminated lung consolidation shadows and ground-glass shadows, and intrapulmonary foci occur at an early time and last a long time. Pulmonary lesions present with rapid progression and could extend rapidly into large patchy and disseminated lesions in a short period. The density change of the lesions, or the mutual transformation between ground-glass change and consolidation density, is also very fast. Besides, imaging signs of acute respiratory distress syndrome may also appear in a short time. Due to the lack of specific diagnostic method of human avian influenza pneumonia, clinical diagnosis entails comprehensive analysis of several examination methods, including epidemiologic history, laboratory examination, chest imaging, and observation of the effects of antibiotics therapy.

The differential diagnosis of human avian influenza pneumonia depends on imaging manifestations combined with the patients' history and clinical and laboratory examinations. Clinically the disease must be differentiated from viral pneumonia such as H1N1 and SARS, mainly from the epidemiological history; laboratory examinations, clinical and imaging characteristics; as well as immune impairment. Their common imaging presentations are ground-glass shadows and pulmonary consolidation shadows, with lesions of rapid change and progression. However, human avian influenza pneumonia demonstrates the fastest progression of the foci and early lesions mainly at the both inferior lung lobes, but such characteristics are not obvious in the case of H1N1 and SARS.

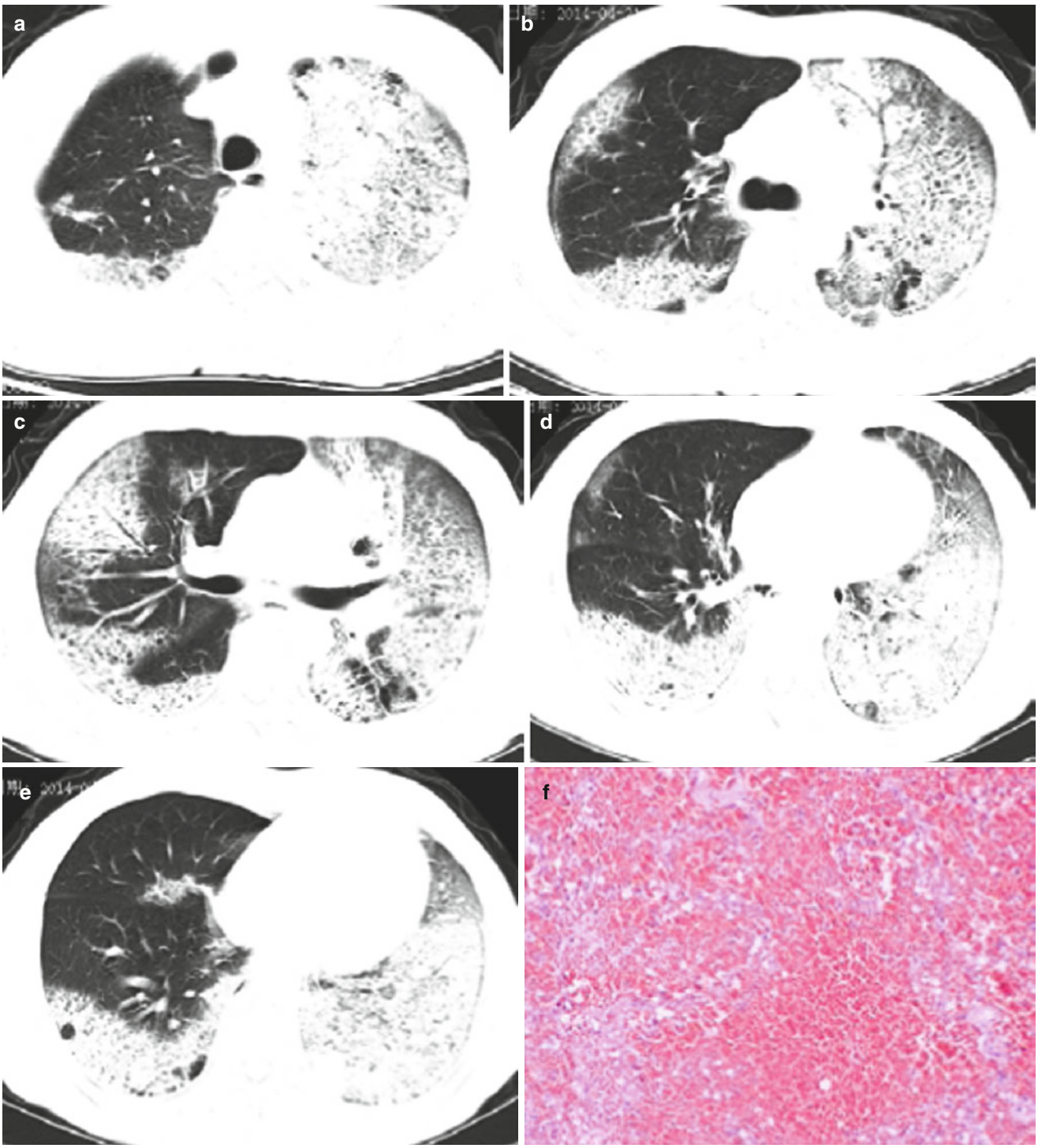

Fig. 3.10 (**a**–**g**) The 50-year-old male patient was confirmed with avian influenza H5N6 pneumonia and received chest CT on April 21, 2014 (the 8th day of onset). (**a**) The left superior lung was detected with large patchy high-density consolidation shadows and apicoposterior segment of right superior lung with patchy shadows at subpleural area. (**b**) The left superior lung was seen with large patchy high-density shadows with air bronchogram in between. The posterior basal segment of right inferior lung lobe and subpleural area of right superior lobe with high-density shadows. (**c**) The inferior layer of the protuberance was revealed with left lung consolidation shadows and right lung superior and middle lobes and the middle and lateral band of the posterior basal segment of right inferior lobe with patchy consolidation shadows. (**d**) For the venous layer of right inferior lung, left lung and right inferior lung were observable with large patchy consolidation shadows, and the subpleura of the right middle lung and right lingula with ground-glass shadows. (**e**) For the diaphragmatic layer, the subpleural area of posterior basal segment of right inferior lobe and left inferior lobe were seen with consolidation shadows, and the subpleural area of the posterior segment of right lung inferior lobe with multiple pulmonary bulla shadows. (**f**) Pulmonary interstitium and alveolar wall capillaries were unveiled with diffusive dilation and congestion accompanied with focal hemorrhage and part of the lung areas with obvious hemorrhage. (**g**) The alveolar cavities were filled with pinkish homogenous effusions, inflammatory cells, and fibrin

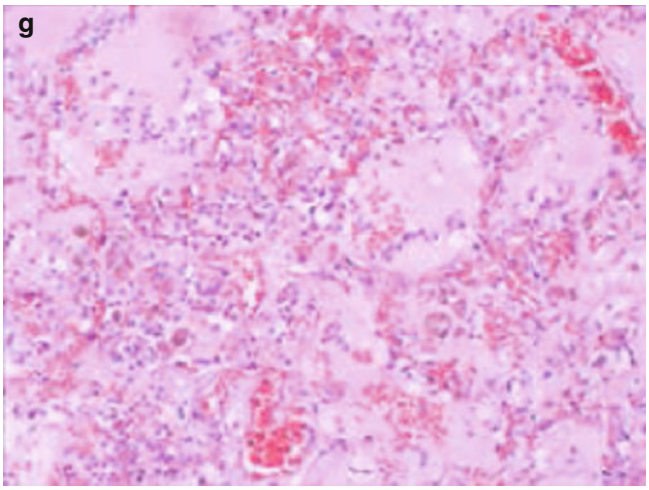

Fig. 3.10 (continued)

3.7.3 Imaging Manifestations of the Complications of Human Avian Influenza Pneumonia

Complication of human avian influenza pneumonia is an important factor affecting the prognosis, which should be highlighted. In the course of treatment of human avian influenza, antivirus drugs, glucocorticoid steroids, and broad-spectrum antibiotics are administered, and positive airway pressure or tracheal cannula may be applied in some patients. Reasonable use of such procedures is of great significance for raising the successful therapeutic rate of patients with human avian influenza pneumonia and lowering mortality rate. However, due to the decrease of the resistance of patients, the drugs and therapies themselves may induce side reactions t and incur corresponding complications. The primary complications of human avian influenza pneumonia encompass secondary lung

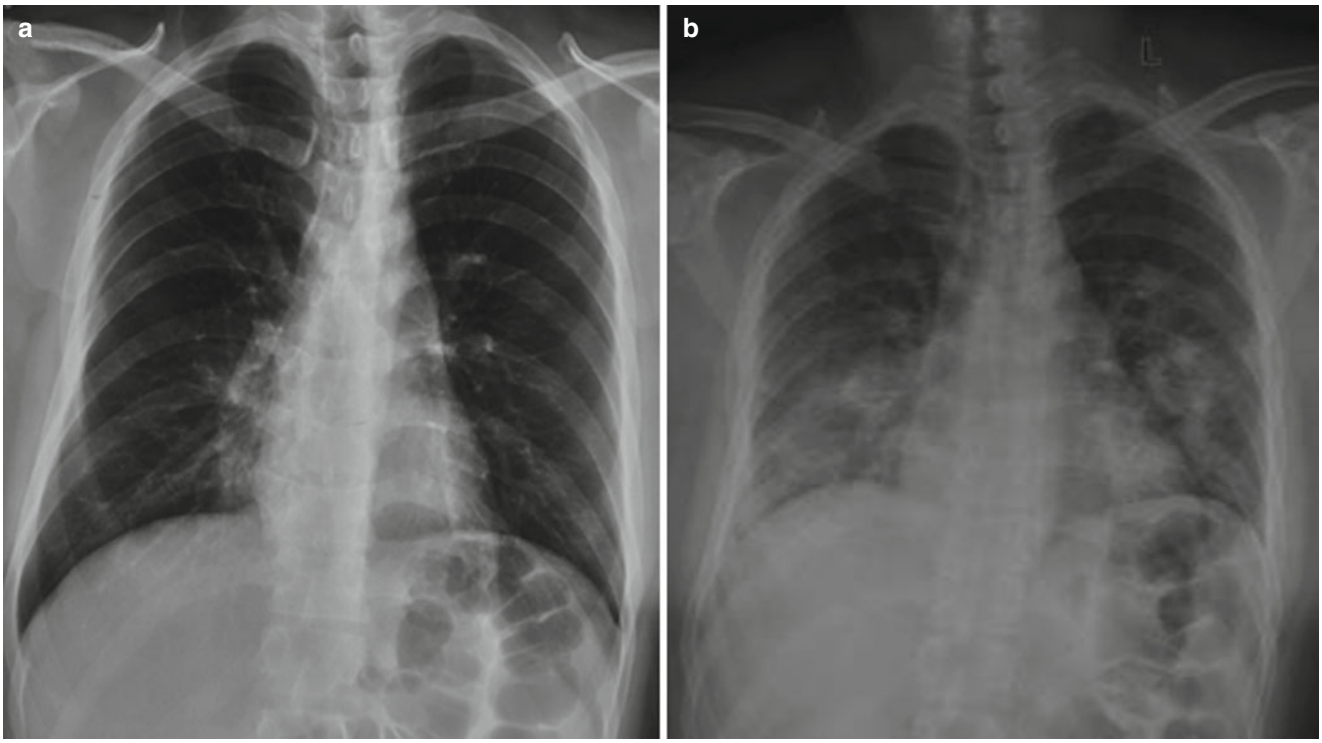

Fig. 3.11 (**a**–**n**) The 31-year-old male patient was confirmed with avian influenza H7N9 pneumonia. (**a**) On the third day after onset of the disease, chest X-ray shows patchy shadows of increased density at mesial margin of the right inferior lung field. (**b**) On the 5th day of the disease onset, chest X-ray visualized large patchy shadows of increased density in the middle and inferior lung fields of both lungs. (**c**–**e**) On the 5th day after the onset of the disease, chest CT demonstrated ground-glass shadows and consolidation shadows scattering at both lungs. Besides, among the consolidation shadows of the right lower lung, air bronchogram was visualized. (**f**–**h**) On the 8th day after the onset of the disease, chest CT revealed extensive ground-glass shadows and consolidation shadows, with the foci increased in number and progressing obviously. (**i**–**k**) On the 11th day after the onset of the disease, after effective treatment, chest CT re-examination disclosed a slight amount of ground-glass density shadows and cord-like and small patchy shadows, indicating entry into recovery phase. (**l**–**n**) On the 15th day after the onset of the disease, chest CT re-examination demonstrated cord-shaped and small patchy shadows, lobular septum thickening, subpleural curvature shadows, bronchiolar dilation, and pleural limited thickening and adhesion at both lungs

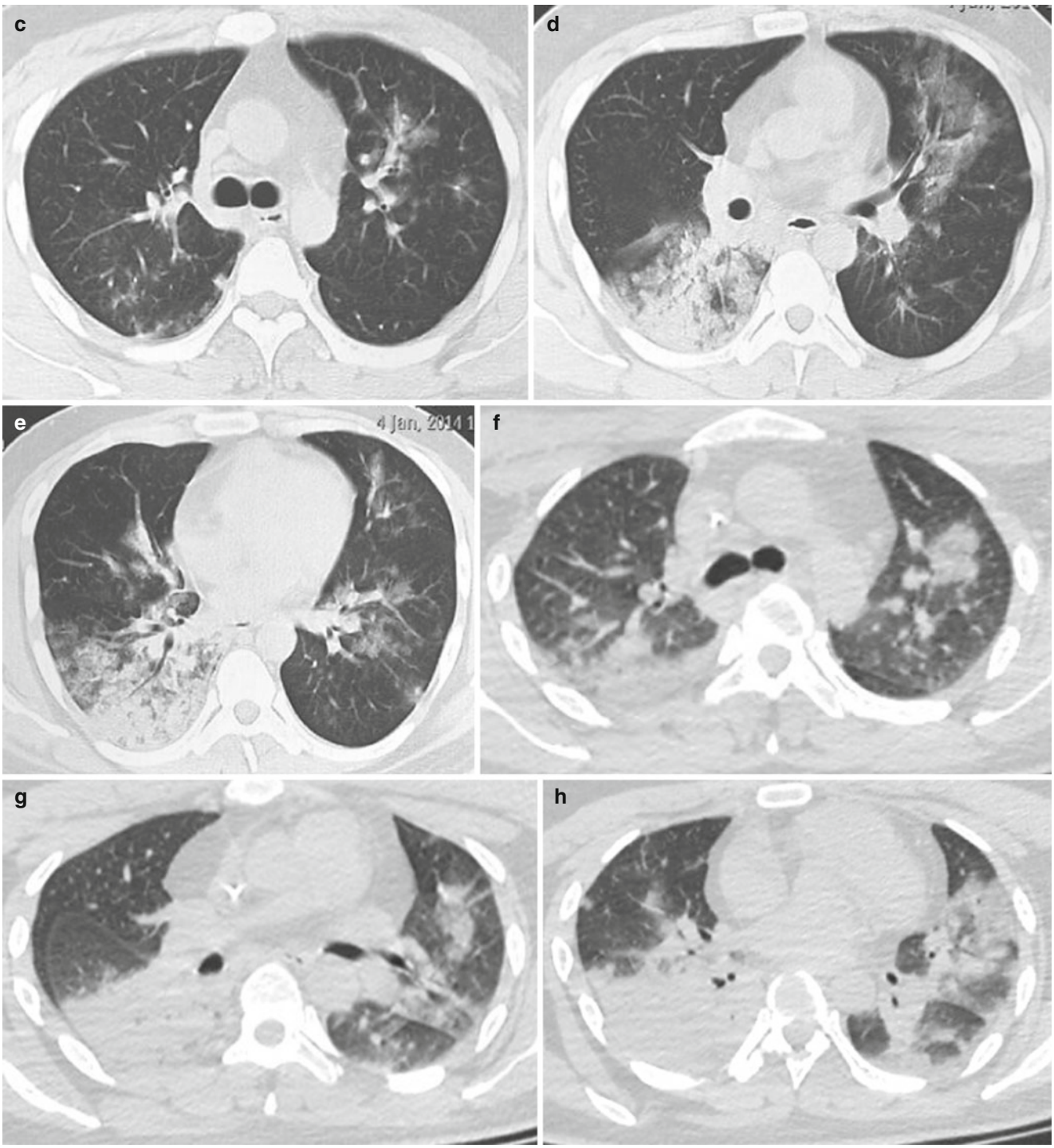

Fig. 3.11 (continued)

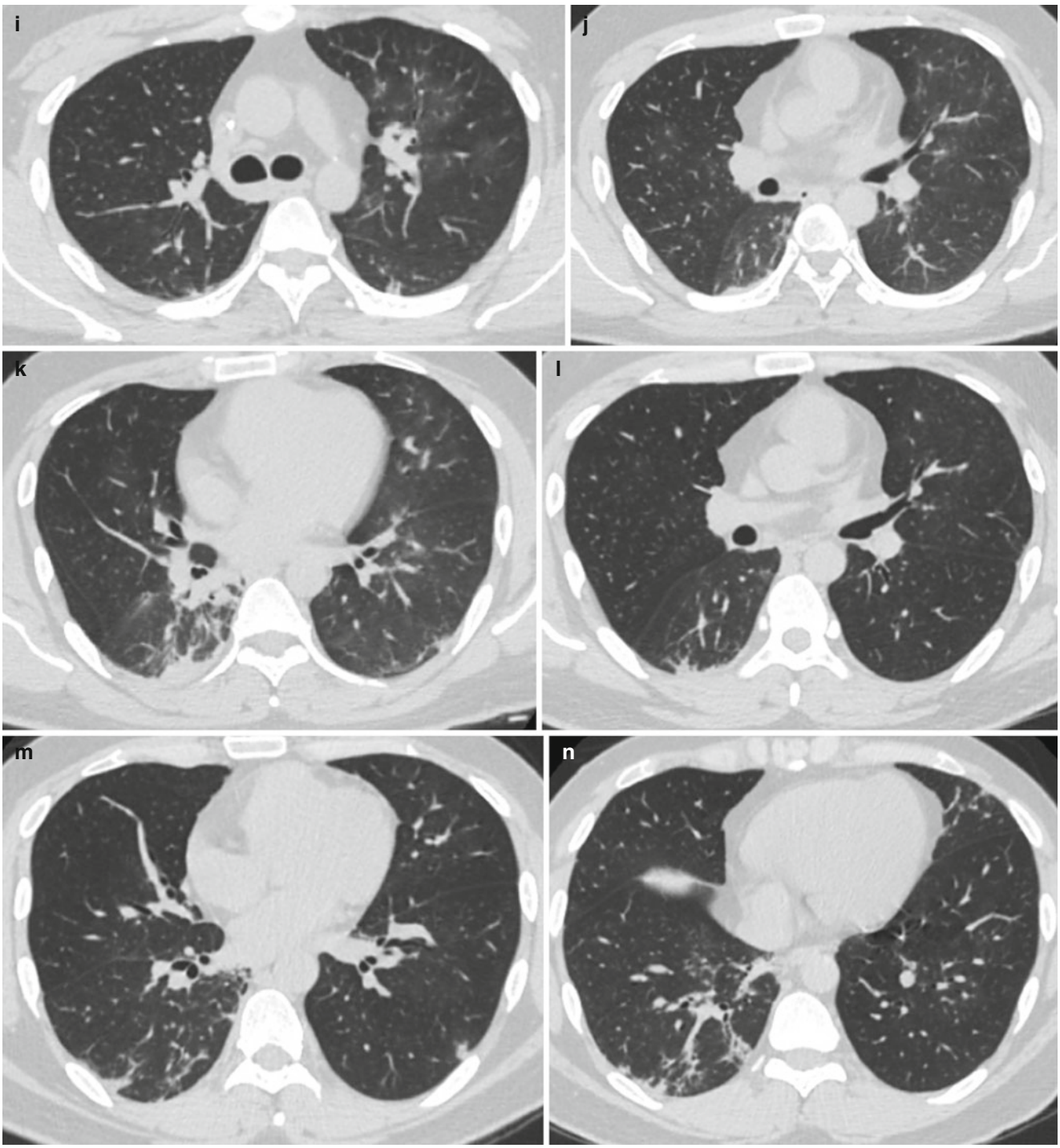

Fig. 3.11 (continued)

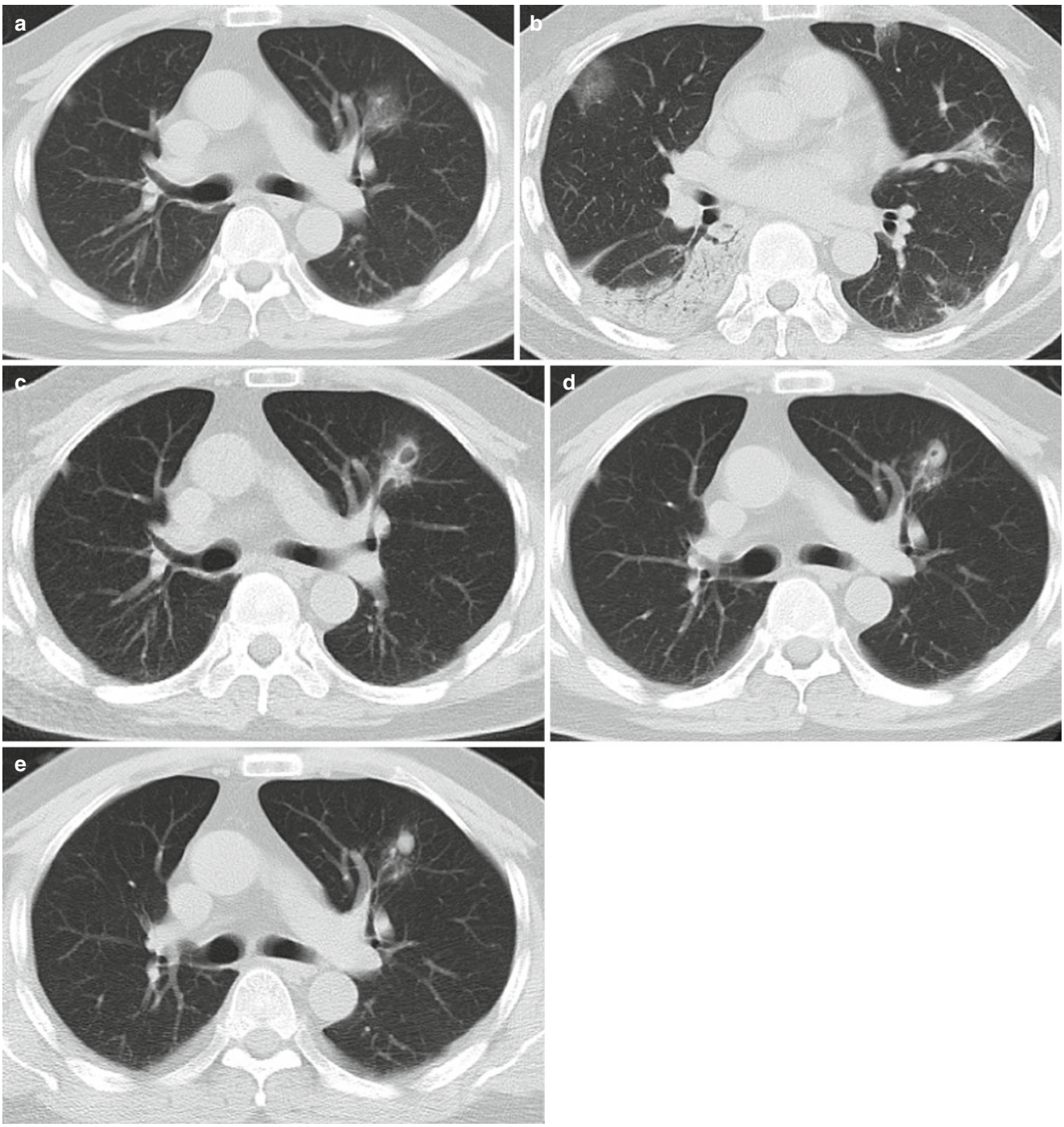

Fig. 3.12 (**a**–**e**) The male patient aged 56 years old was diagnosed with avian influenza H7N9 pneumonia. (**a**, **b**) On the 6th day after onset of the disease, chest CT scan demonstrated consolidation shadows and air bronchogram at the right inferior lung lobe and scattering patchy ground-glass shadows at the right middle lobe and subpleural area of the left lung. (**c**) On the 22nd day after the onset of the disease, chest CT showed absorption of the majority of right inferior lung consolidation shadows and presence of small lung air sacs at left superior lung with relatively clear inner wall. (**d**) On the 26th day after the onset, chest CT suggested absorption of small pulmonary air sacs at left superior lung. (**e**) On the 43th day after the onset of the disease, chest CT indicated basal absorption of small lung air sacs at left superior lung and presence of nodular shadows

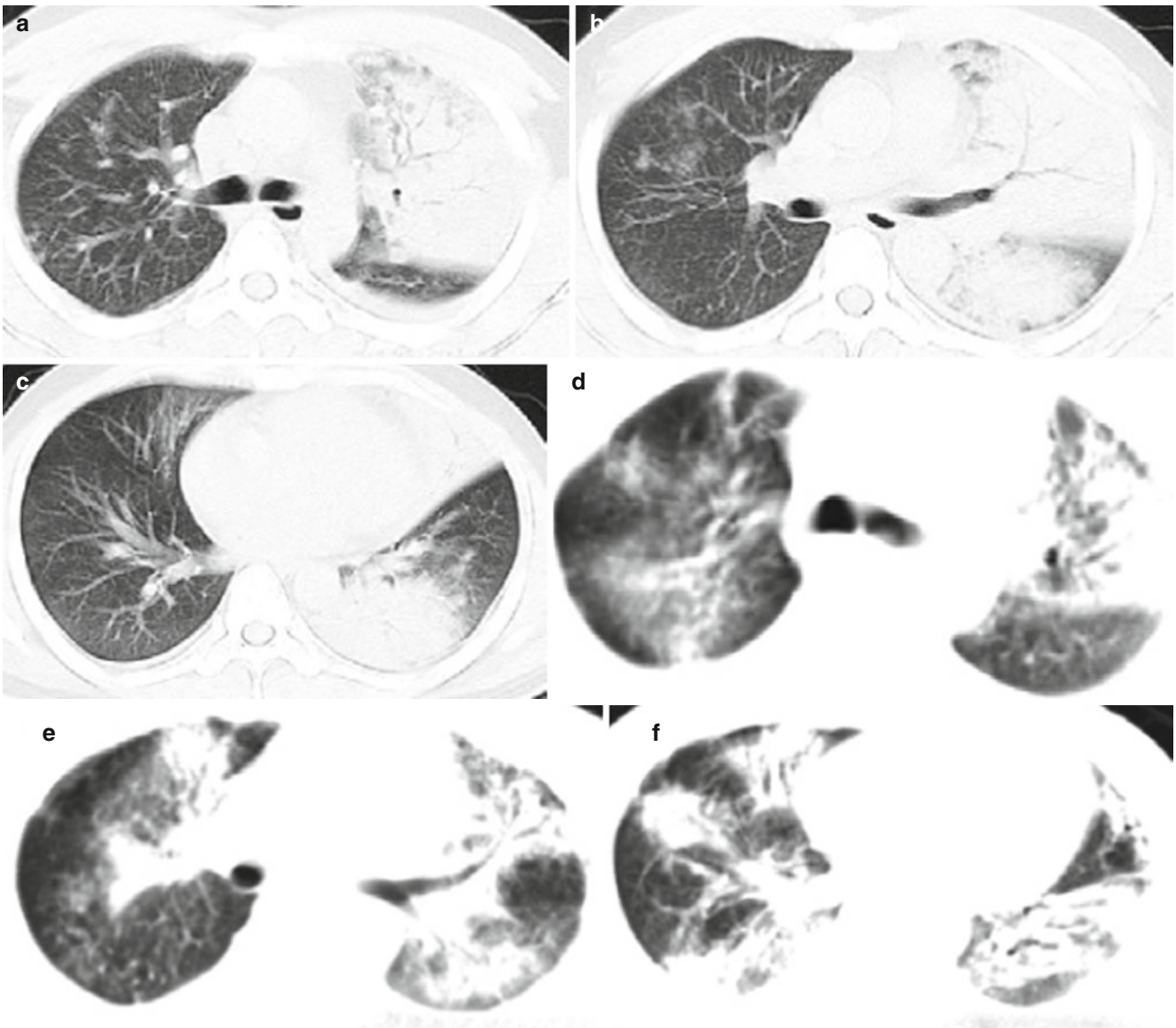

Fig. 3.13 (**a**–**u**) The male patient aged 31 years old was confirmed with human avian influenza subtype H5N1severe pneumonia complicated by ARDS. (**a**–**c**) On the 9th day after the onset of the disease, chest CT showed large patchy consolidation shadows at the left lung, with air bronchogram observable in between. The right lung was seen with scattered patchy ground-glass shadows. (**d**–**f**) On the 34th day after the onset of the disease, both lungs were found with extensive consolidation shadows and ground-glass shadows; the left lung presented mainly consolidation shadows and air bronchogram. There were shrinkage of left inferior lobe and aggregation of lung texture. (**g**–**i**) On the 96th day after the onset, both lungs were visualized with patchy inhomogeneous consolidation shadows and cord-like shadows, with patchy ground-glass shadows seen peripheral to consolidation shadows at both lungs. (**j**–**l**) On the 286th day after the onset of the disease, CT revealed that foci of both lungs were predominated by pulmonary interstitial changes such as fibrous cord-like and latticed shadows, with concurrent ground-glass shadows. Absorption of the foci slowed down distinctly. (**m**–**o**) 2 years after onset of the disease, CT unveiled fibrous strip and latticed shadows in both lungs, and patchy ground-glass shadows at the left superior lung and bilateral inferior lungs. Compared with the chest CT presentations 1 year before, the foci were slightly absorbed. (**p**–**s**) 39 months after the onset of the disease, chest CT suggested fibrous strip and latticed shadows at bilateral superior lungs as well as thickening of interlobular septum, paramediastinal emphysema, small consolidation shadow, and signs of bronchiectasis. The left superior and right inferior lung were detected with small patchy ground-glass shadows. (**t**–**u**) 5 years and 7 months after the onset of the disease, both lungs were visualized still with fibrous strip shadow, latticed shadow, and bronchiectasis signs, particularly at the right middle lobe and left superior lobe. Both lungs were found with small consolidation shadows and small patchy ground-glass shadows

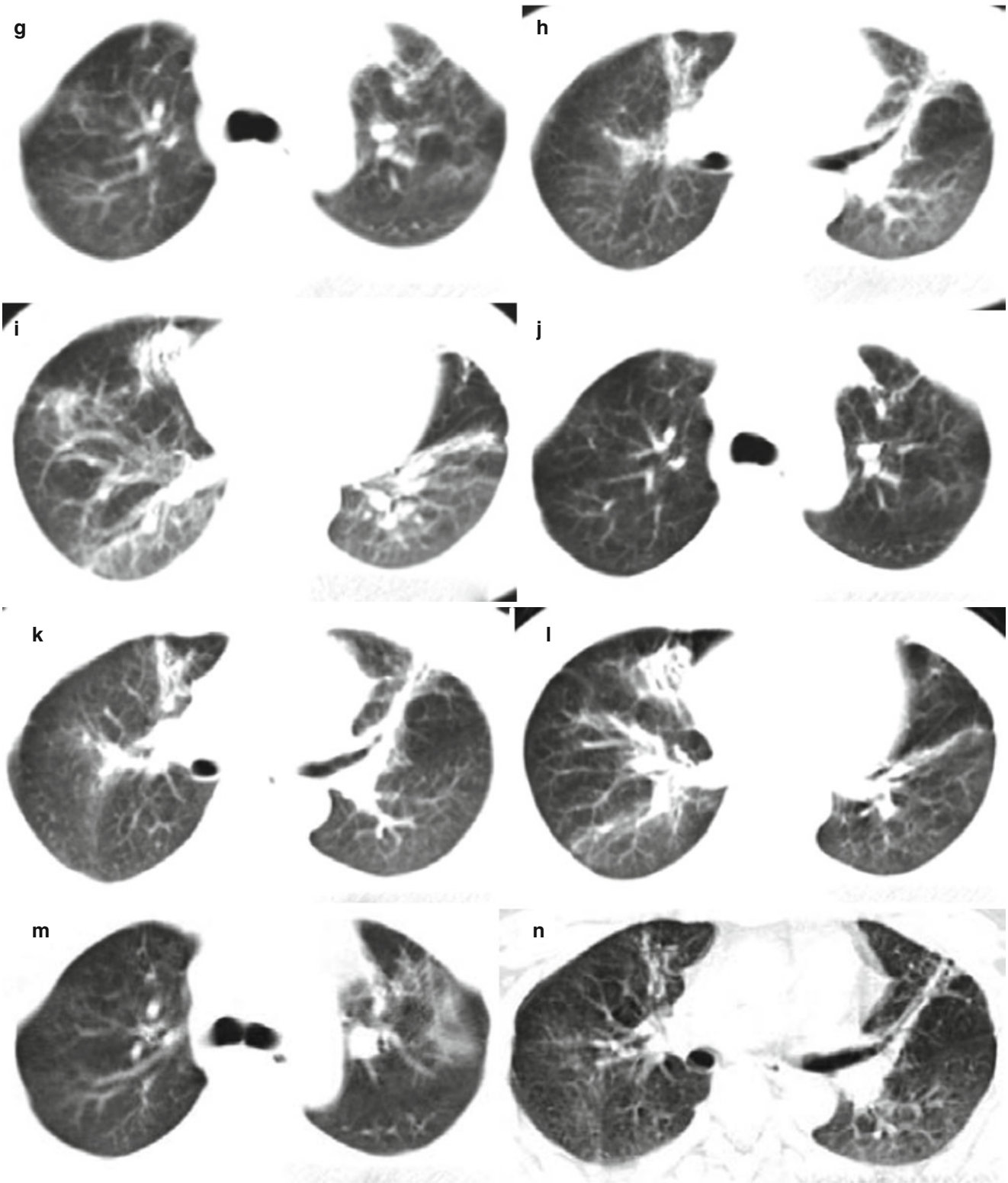

Fig. 3.13 (continued)

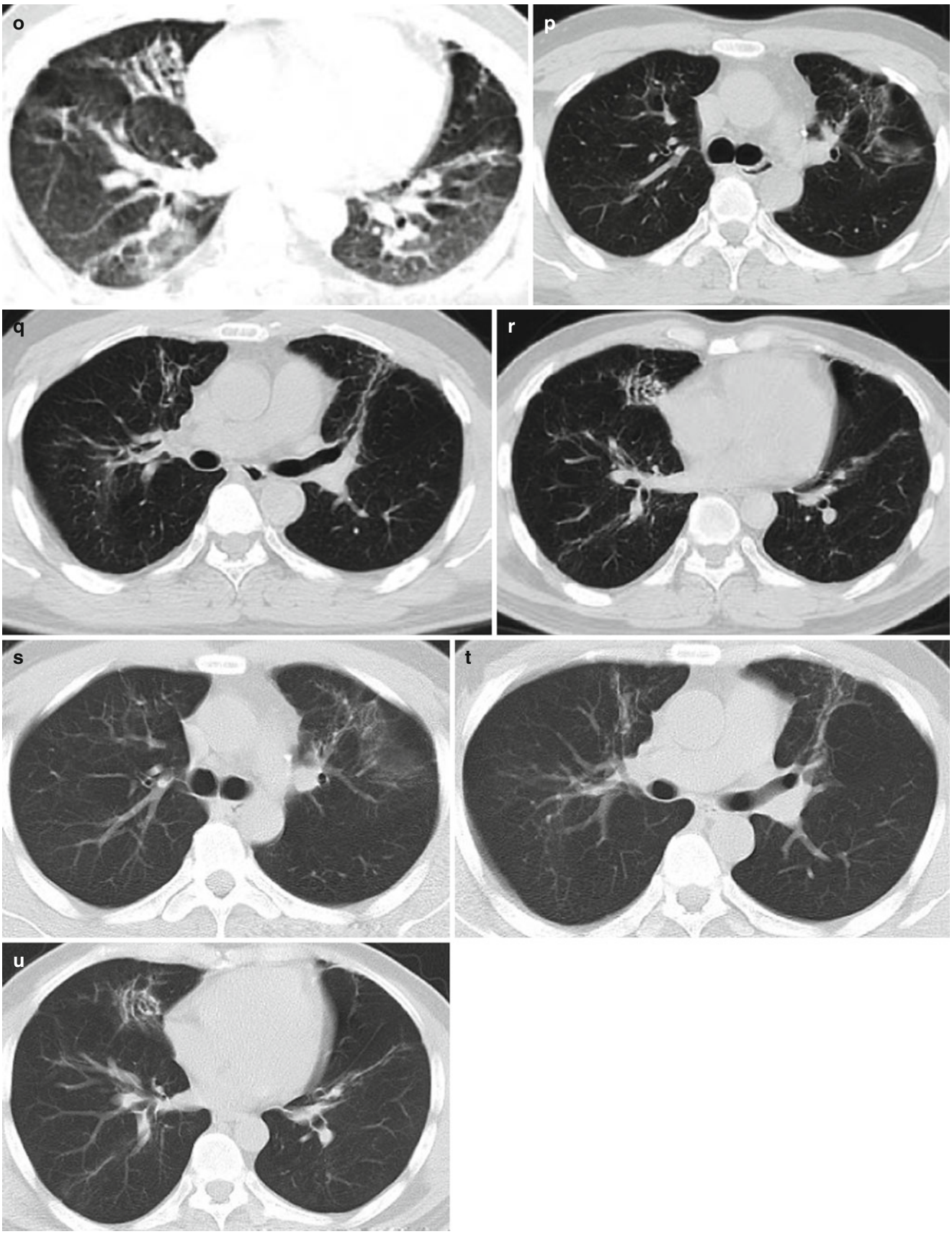

Fig. 3.13 (continued)

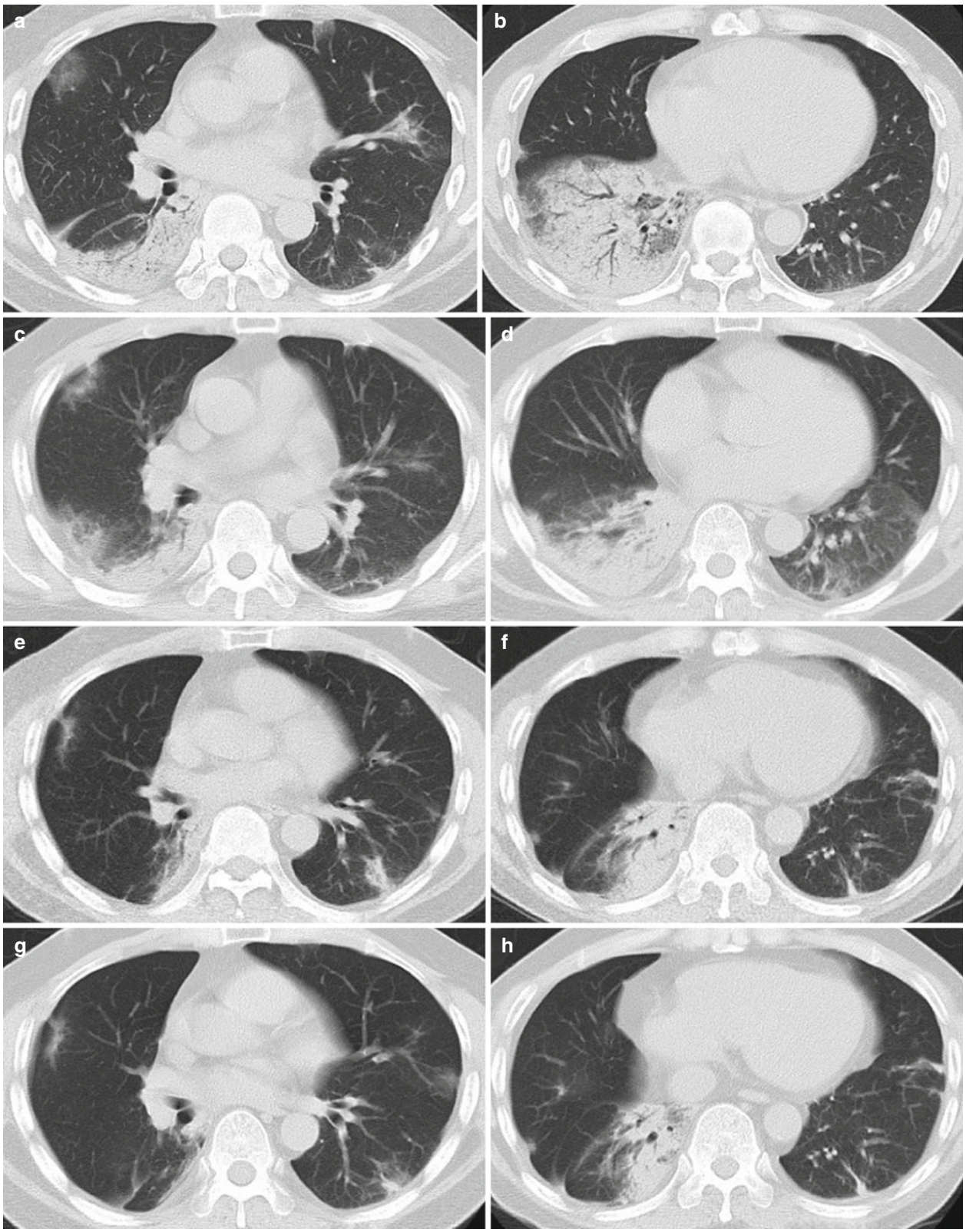

Fig. 3.14 (**a**–**h**) The 56-year-old male patient was detected with avian influenza H7N9 pneumonia. (**a**, **b**) On the 6th day after the onset of the disease, chest CT indicated large patchy consolidation shadows at right inferior lung lobe accompanied by air bronchogram. The right middle lobe and subpleural area of left lung were visualized with scattered patchy ground-glass shadows. (**c**, **d**) On the 13th day after the onset of the disease, chest CT suggested absorption of large patchy consolidation shadows at the right inferior lung lobe. The left inferior lung was found with ground-glass shadows. (**e**, **f**) On the 21st day after the onset of the disease, chest CT demonstrated obvious absorption of large patch of consolidation at right lung lobes. (**g**, **h**) On the 25th day after the onset of the disease, chest CT revealed fibrous strip shadows at the right lung lobes. The left lung and right superior lung presented with absorption of the patchy ground-glass shadows

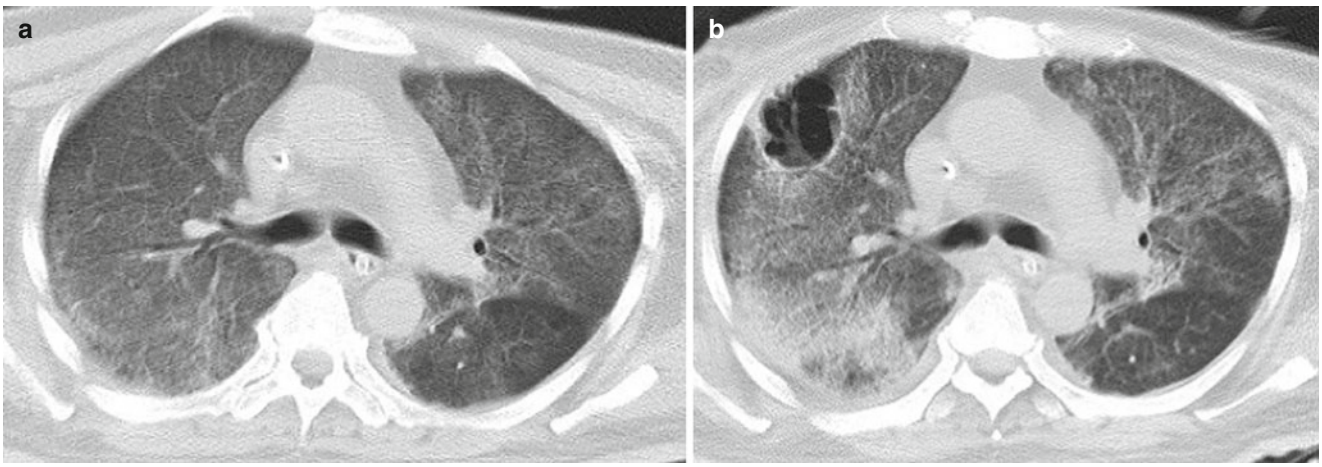

Fig. 3.15 (**a**, **b**) The male patient aged 48 years old was diagnosed with avian influenza H7N9 severe pneumonia accompanied by *Acinetobacter baumannii* infection. (**a**) On the 15th day after the onset of the disease, both lungs were revealed with ground-glass-density shadows and the original right inferior lung consolidation shadows were basically absorbed. Avian influenza virus H7N9 became negative. (**b**) On the 24th day after onset of the disease, the patient suffered from fever, and culture of deep sputum for two times showed *Acinetobacter baumannii*. CT visualized consolidation shadows at the right lung and small patchy consolidation shadow at the subpleural area of the left superior lung

infection, mediastinal and subcutaneous emphysema, pneumothorax, lung fibrosis, and nonbacterial necrosis of the head of the femur. These complications or sequelae are also discovered mainly by imaging. Knowledge about human avian influenza imaging presentations could help elevate the curative rate and decrease mortality of human avian influenza.

3.7.3.1 Lung Secondary Infections

Pathogenesis

Human avian influenza virus may attack the human immunity system directly and compromise immunity.

Large doses of glucocorticoids are administered during treatment which could undermine the immunity.

Some patients may still need such treatment as positive airway pressure or bronchial intubation and central venous indwelling catheter, which create conditions for secondary infection.

Meanwhile, abundant use of broad-spectrum antibiotics could disturb the normal bacterial flora. The most frequent and severe is a complication with *Acinetobacter baumannii* infection.

Clinical and Imaging Diagnosis of Complication of *Acinetobacter baumannii* Infection

Acinetobacter baumannii is highly capable of acquiring drug tolerance and clone dissemination, and *Acinetobacter baumannii* with multiple drug tolerance and broad drug tolerance is one of the most important pathogen of human avian influenza. *Acinetobacter baumannii* may induce nosocomial pneumonia, bloodstream infection, abdominal infection, central nervous system infection, urinary system infection, cutaneous soft tissue infection, and myelitis. The diagnosis may be concluded based on following evidences: (1) besides clinical symptoms, signs and imaging presentations consistent with pneumonia, new or sustained or aggravated lung exudates, infiltration, and consolidation are detected (Fig. 3.15). (2) Host factors including underlying disease, immune status, application of antibacterial medicines in early period, and duration of mechanical ventilation (3).

Sputum culture for over two times shows growth of pure *Acinetobacter baumannii* or dominant growth of *Acinetobacter baumannii*; or blood culture demonstrates with growth of *Acinetobacter baumannii*.

3.7.3.2 Mediastinal and Subcutaneous Emphysema

All patients with avian influenza suffer from different degrees of lung fibrosis and lung impairment, and the majority of patients need assisted respiration such as artificial assisted ventilation of the ventilator and tracheotomy intubation, which could heighten intrapulmonary pressure by different degrees. However, as patients with human avian influenza manifest varying degrees of inflammatory exudation from lung tissues, the occlusive fibrosis inside bronchioli may lead to rupture of alveolar elastic fibers, which may on one hand damage lung air exchange and on the other hand lower lung compliance. Under the condition of increased intrapulmonary pressure, pneumothorax and mediastinal and subcutaneous emphysema are more likely to occur.

Imaging presentations: CT suggests air-density linear shadows encircling the mediastinum and shift of the mediastinal pleura toward lung field. Air in the mediastinum escapes along the cervical fascial space to the neck and chest subcutaneous area, thus rendering subcutaneous gas-density imaging signs (Figs. 3.3, 3.4, 3.5, 3.6, 3.7, 3.8, 3.9, 3.10, 3.11, 3.12, 3.13, 3.14, 3.15, and 3.16).

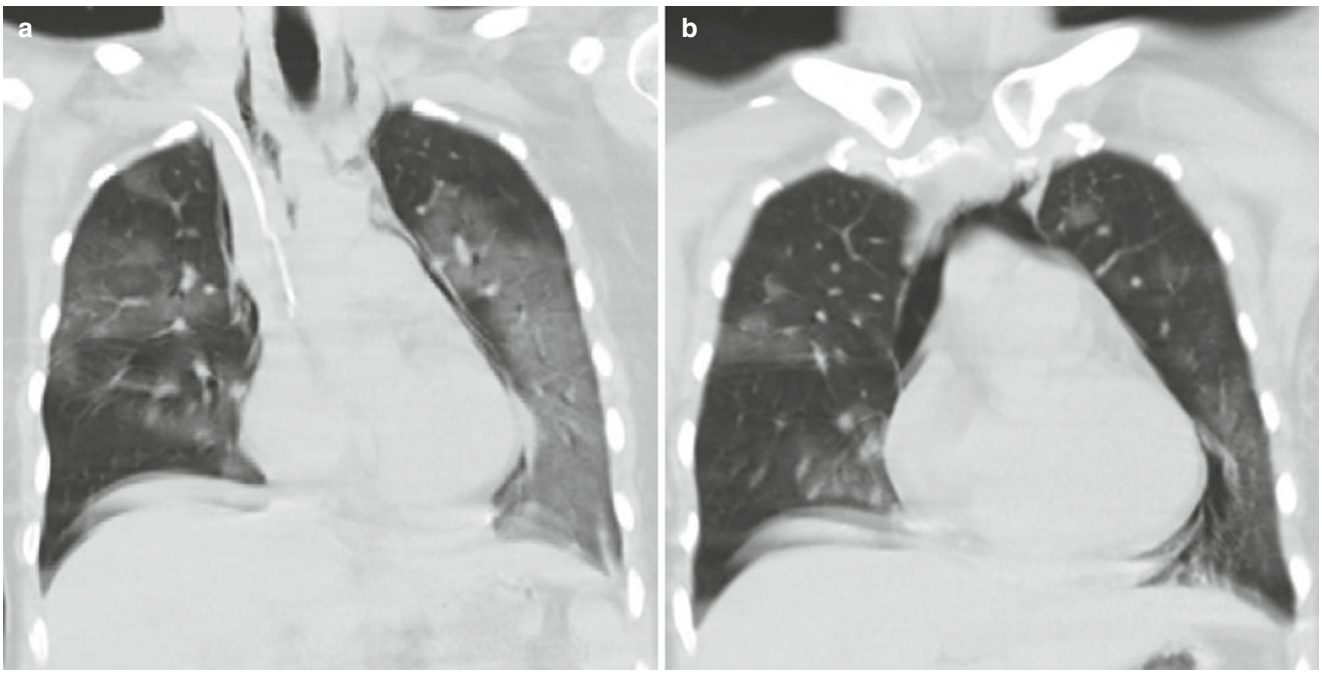

Fig. 3.16 (**a**, **b**) The 34-year-old male patient was diagnosed with avian influenza H7N9 severe pneumonia complicated with mediastinal pneumatosis. Coronal imaging visualized remarkable pneumatosis at the neck, mediastinum, and the periphery of the heart and large blood vessels

3.7.3.3 Lung Interstitial Fibrosis

Pathologic Basis of Clinical Imaging

In the early phase of onset, human avian influenza presents with bronchiolar and peripheral parenchymal or interstitial lesions, which may progress into alveolar parenchymal and interstitial lesions, mostly reversible. In the phase of recovery, some cases may advance into pulmonary interstitial proliferation and then into fibrosis. The degree and outcome of lung interstitial proliferation and fibrosis are related to the scope of lung involvement in the climax phase, presence of complications, as well as treatment.

Imaging Manifestations

The initial signs of lung interstitial proliferation are thickening of lobular septum and intralobular interstitium as well as subpleural curvature shadows. The intrapulmonary patchy become smaller and denser, and high-density cord and honeycomb-like shadows are gradually observable in the lungs. Severe lung interstitial proliferation could make the lungs shrink and mediastinum shift toward the affected side. Lung interstitial proliferation may exist extensively in the lungs, predominated by thickening of interlobular septum and interlobular interstitium as well as subpleural curvature imaging changes. It may also manifest local irregular high-density plaque and cord-shaped shadows. Intrapulmonary honeycomb-like imaging presentation and traction bronchiectasis are primary signs of lung interstitial fibrosis.

CT reveals cord-like, reticular, and honeycomb-shaped shadows. HRCT could better display the meticulous abnormal changes of pulmonary interstitium, such as thickening of lobular septum, intralobular interstitial thickening, subpleural curvation shadow, honeycomb-like shadow, paraseptal emphysema, as well as bronchiolar dilatation (Figs. 3.17 and 3.18).

3.7.3.4 Ischemic Necrosis of Femoral Head and Osteomyelitis

Pathogenesis

TAt present its pathogenesis still remains unclear and it might be associated with the inflammatory reaction and damage from use of hormones and human avian influenza combined with bacterial infection (such as *Acinetobacter baumannii* infection) or multiple mixed factors on sclerotin and blood vessels. Femoral head aseptic necrosis is typical of degenerative changes due to femoral head blood circulation disturbance, with limping and pain as main symptoms. The affected lower limb is slightly shorter and manifests mild flexion and adduction. The abduction and intorsion slightly limited.

Imaging Presentations of Aseptic Necrosis of the Femoral Head

In the early phase of femur head aseptic necrosis, CT demonstrates that the stellate sign formed by femoral trabeculae become deformed or disappeared, visualized as spot or patchy shadows with increased density in the femoral head and tuft-

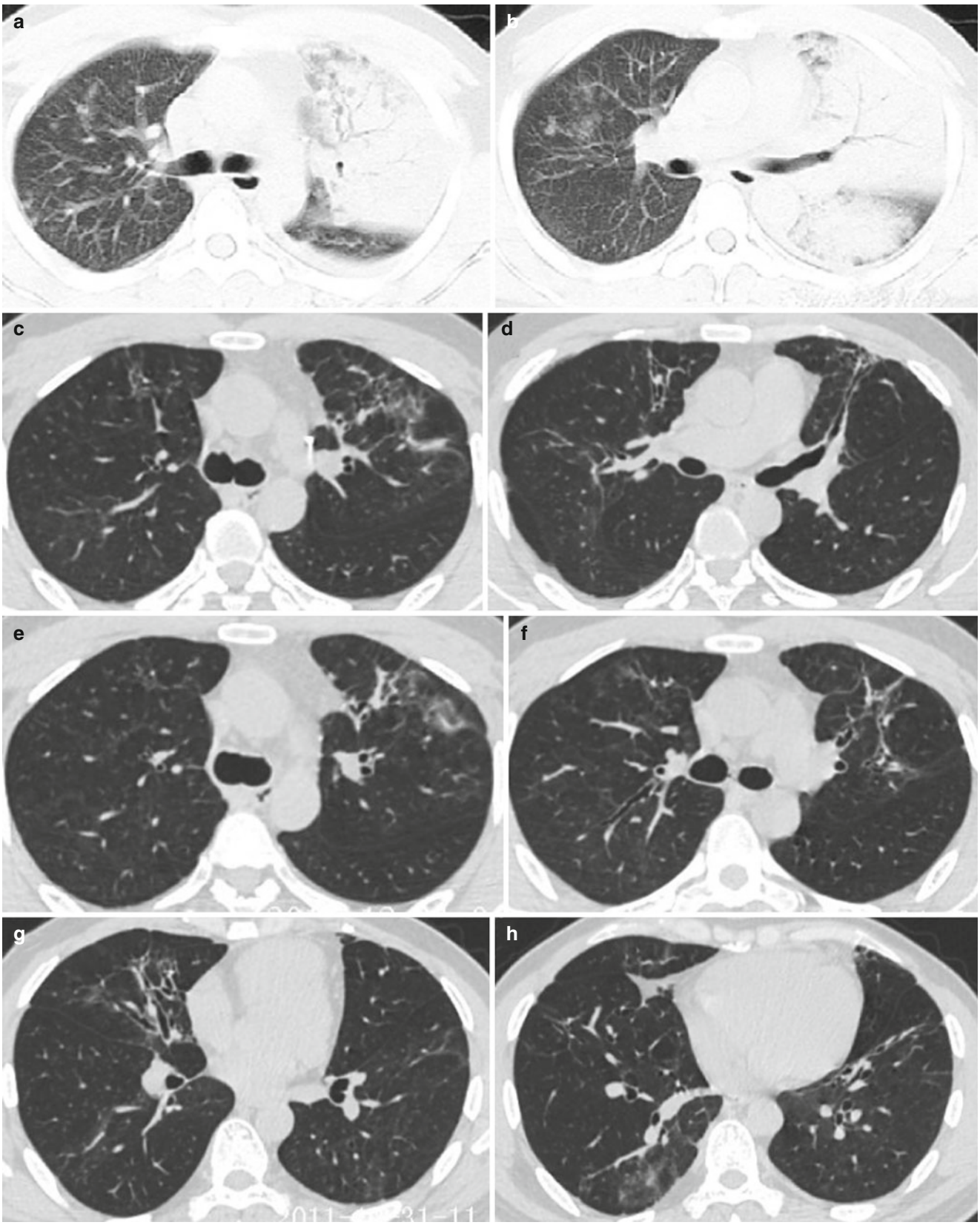

Fig. 3.17 (**a**–**j**) The male patient aged 34 years old was confirmed with human avian influenza H5N1 complicated by pulmonary interstitial fibrosis. (**a**, **b**) On the 9th day after the onset of disease, chest CT suggested large patchy consolidation shadows, with air bronchogram in between. The right lung was seen with scattered ground-glass shadows. (**c**, **d**) 5 years and 7 months after onset of the disease, chest CT follow-up revealed fibrous strip shadows and latticed shadows at both lungs as well as bronchiectasis. (**e**–**g**) The left lung ligule and right inferior lung middle lobe were detected with small patchy ground-glass shadows, fibrous strip shadows, and bronchiectasis. (**h**, **i**) The inferior lobes of both lungs were unveiled with strip consolidation shadows, small patchy ground-glass shadows, and paraseptal emphysema. (**j**) The coronal view of three-dimensional construction suggested a quasi-circular nodular shadow in a diameter of about 2 mm in left main bronchus

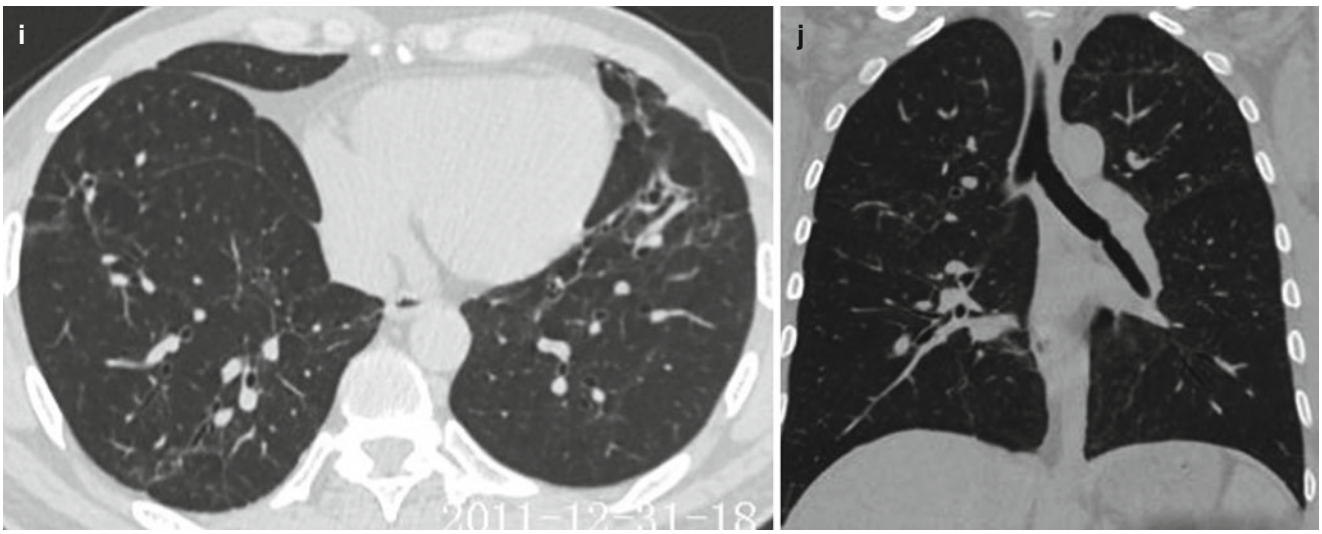

Fig. 3.17 (continued)

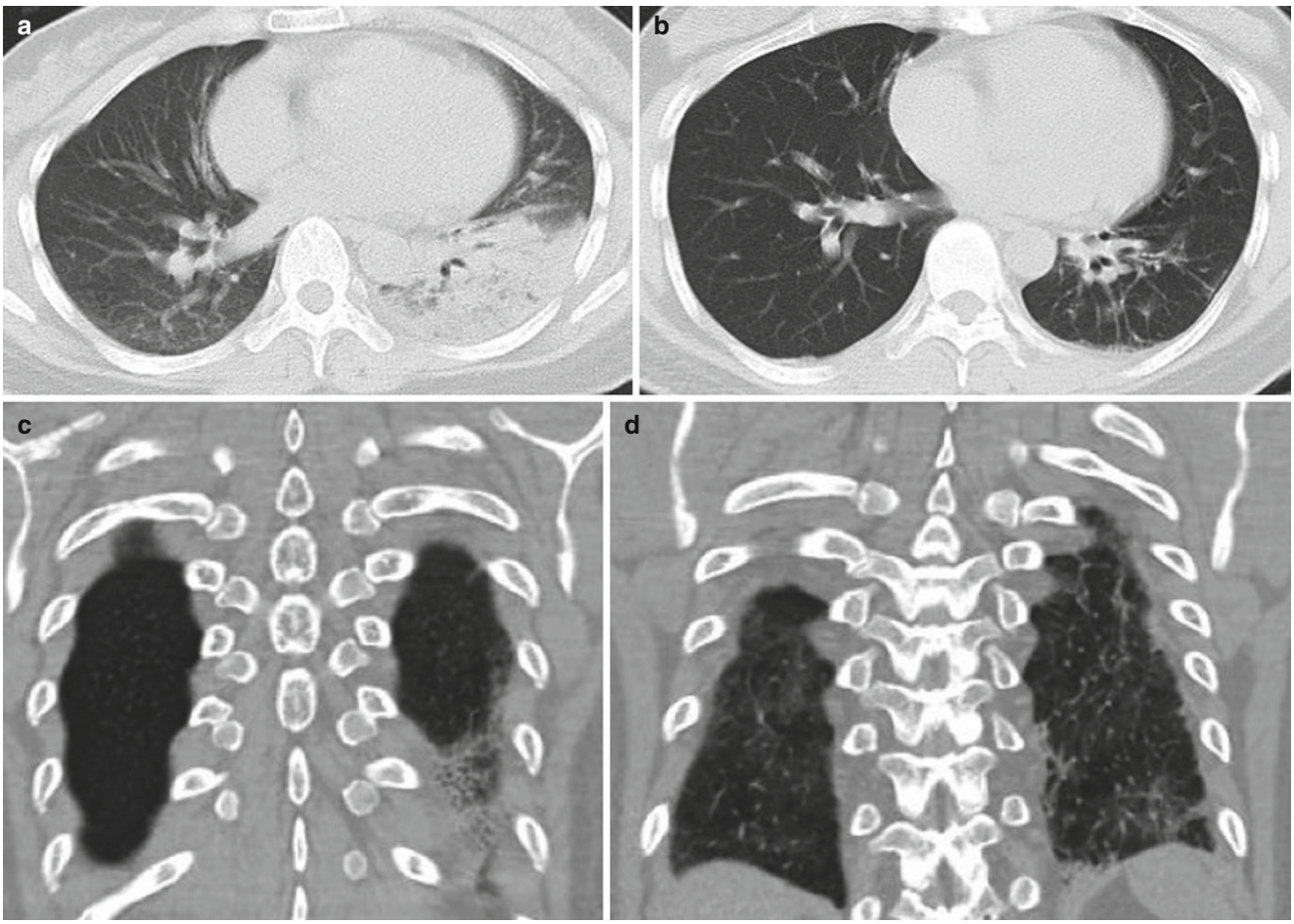

Fig. 3.18 (**a**–**e**) The female patient aged 43 years old was identified with avian influenza H7N9 severe pneumonia complicated by lung interstitial fibrosis. (**a**) On the 10th day after the onset of the disease, chest CT showed large patchy consolidation shadows at the right inferior lung. (**b**) On the 34th day after the onset of the disease, the transverse image of chest CT re-examination indicated fibrous strip shadows and subpleural curvature shadows. (**c**) Coronal view of three-dimensional reconstruction found mosaic sign at the left inferior lung. (**d**) Coronal view of three-dimensional reconstruction demonstrated extensive pulmonary interstitial proliferation at the dorsal sides of both lungs. (**e**) Coronal view of three-dimensional reconstruction unveiled emphysema at the right superior paramediastinum, and cord-like shadow at the right inferior lung; and bronchiectasis sign at the left inferior lung

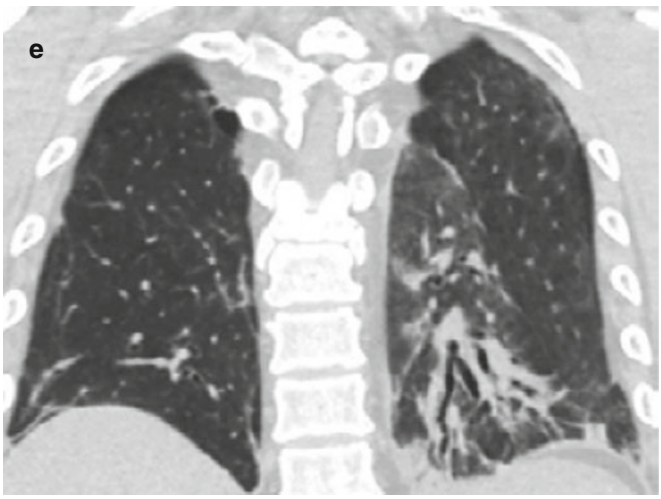

Fig. 3.18 (continued)

shaped change or mutual fusion at the periphery of stellate sign. In the advanced phase, the femur head becomes fragmented and deformed, and the absorption of sclerotin between fragmented bones presents irregular low-density area, with the stellate sign absent. Based on MRI presentations, aseptic necrosis of the femur head may be divided into the following four phases: Phase I shows homogenous or inhomogeneous low-signal areas adjacent to joints above the femur head on weighted T1 and T2 imaging; phase II manifests wedge-shaped mixed low-signal band; phase III is typical of sequestrum crescent sign and cortical collapse; phase IV manifests phase III signs accompanied by joint degeneration and joint space stenosis.

Besides, apart from the most common ischemic necrosis of the femoral head, osteomyelitis is also documented, mostly at the femur, which presents irregular low-signal area on T2 weighed imaging (Fig. 3.19).

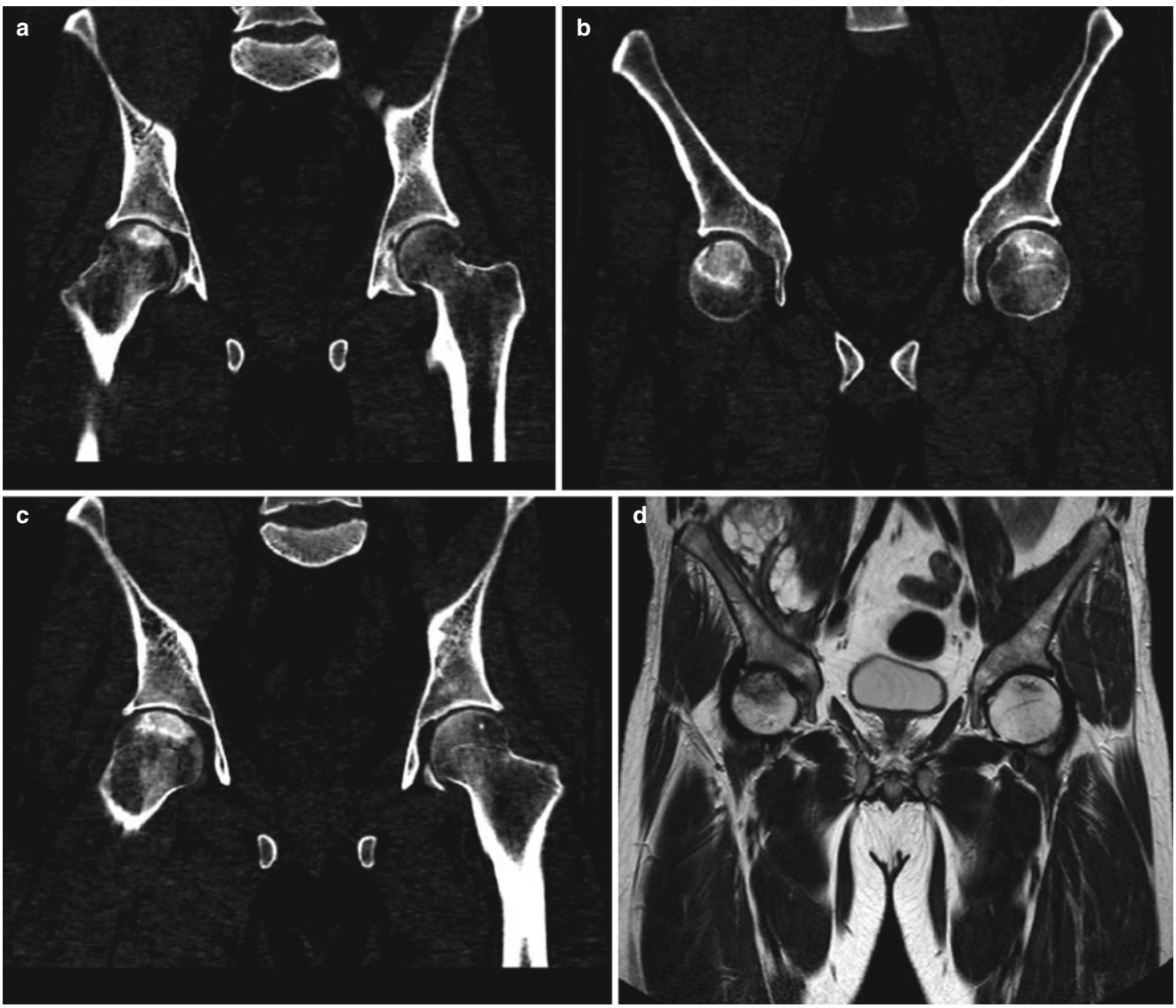

Fig. 3.19 (**a**–**g**) The 39-year-old male patient was detected with avian influenza H7N9 severe pneumonia accompanied by bilateral femur head ischemic necrosis and osteomyelitis of the middle and upper segment of the left and right femurs. (**a**–**c**) On the 27th day after onset of the disease, pelvic CT plain scan coronal view revealed patchy shadows of increased density at bilateral femur heads, prominently at the right femoral head. (**d**–**g**) On the 37th day after onset of the disease, pelvic MRI plain scan disclosed the bilateral femoral heads of irregular low signals on weighted T1 and T2 imaging, and the middle and upper segments of the left and right femur with irregular low signals on weighted T2 imaging

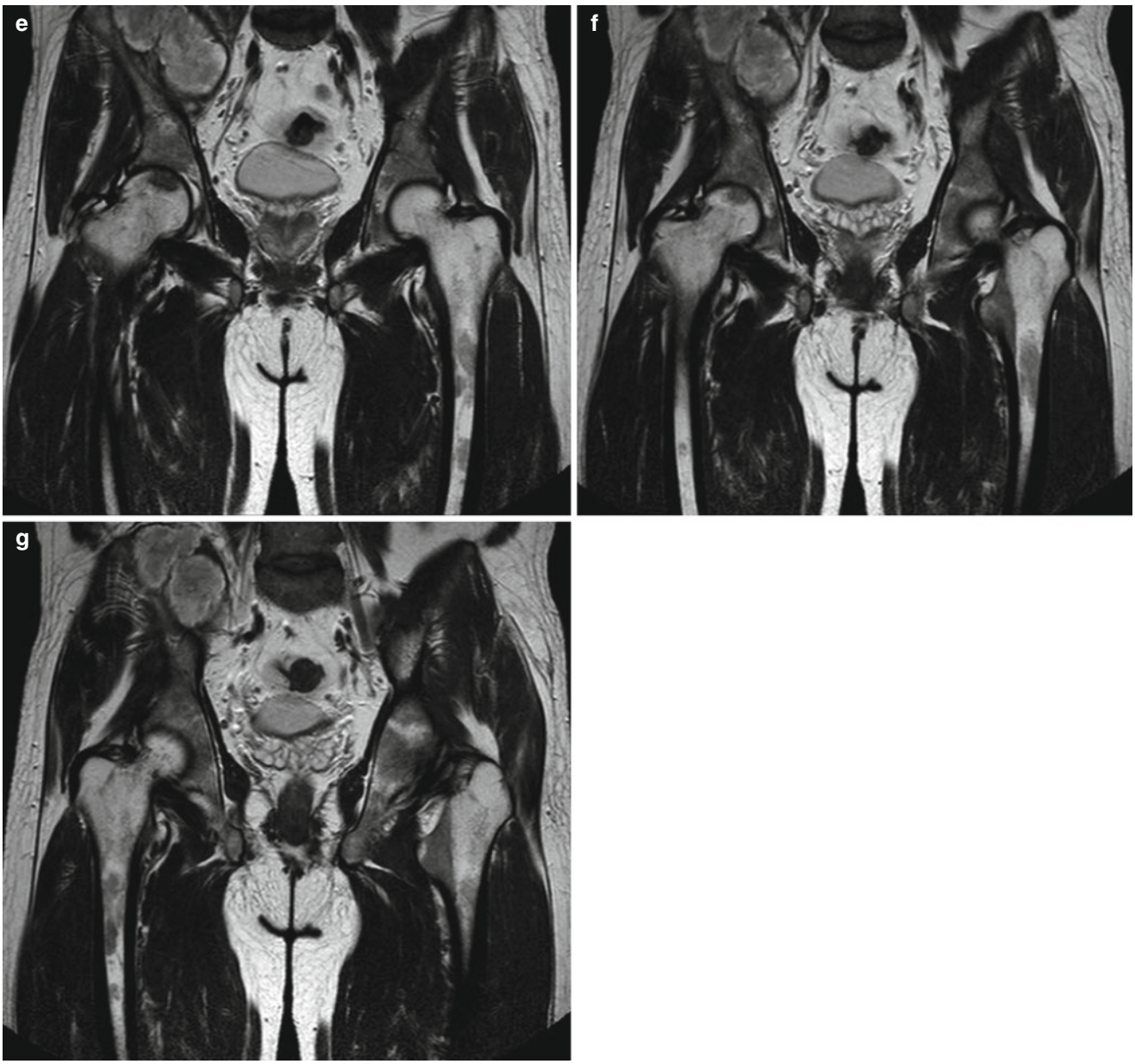

Fig. 3.19 (continued)

Further Reading

1. Luo RP, Zhu YM, Xu ZY, et al. Report of the first human case of H5N1 avian influenza pneumonia in China mainland. Chin J Pediatr. 2006;44(5):342–5.
2. Xu XY, Wang QY. Biology and epidemiology of human avian influenza. Nat Med J Chin. 2004;84(5):342–5.
3. Huang XR, Zeng Z, Lu PX, et al. Clinical Imaging Analysis of 12 cases of human avian influenza H7N9 pneumonia [J]. Chin J CT MRI. 2014;12(2):8–11.
4. Henter JI, Chow CB, Leung C, et al. Cytotoxic therapy for severe avian influenza A (H5N1) infection. Lancet. 2006;367(9513):870–3.
5. Ungchusak K, Auewarakul P, Dowell SF, et al. Probable person-to-person transmission of avian influenza A (H5N1). N Engl J Med. 2005;352(4):333–40.
6. Lin J, Zhang J, Dong X, et al. Safety and immunogenicity of an inactivated adjuvanted whole-virion influenza A(H5N1) vaccine: a phase I randomised controlled trial. Lancet. 2006;368(9540):991–7.
7. Oner AF, Bay A, Arslan S, et al. Avian influenza A (H5N1) infection in eastern Turkey in 2006. N Engl J Med. 2006;355(21):2179–85.
8. Obenauer JC, Denson J, Mehta PK, et al. Large-Scale Sequence analysis of avian influenza isolates. Science. 2006;311(5767):1576–80.
9. Li Q, Lan Y, Xu CL, et al. Study on a deceased pregnant patient with avian influenza (H5N1) [J]. Chin J Epidemiol. 2006;27(4):288–92.
10. Zhou BP, Yi-min LI, Lu PX. Human avian influenza. Peking: Science Press; 2007.
11. Yu HJ, Chen YX, Shu YL, et al. Investigation and confirmation of the first case of human avian influenza H5N1 in China mainland. Chin J Epidemiol. 2006;27(4):281–7.
12. Bai YQ, Xu G, Gong ZL, et al. Autopsy pathological analysis of human highly pathogenic avian influenza H5N1. Chin J Pathol. 2006;32:545–8.
13. Beigel JH, Farrar J, Han AM, et al. Avian influenza A (H5N1) infection in human. N Engl J Med. 2005;353(13):1374–85.

14. Zhang W*, Wen LY, Lu M, et al. Clinical characteristics of the first human highly pathogenic influenza H_5N_1 in Jiangxi Province. Chin J Tuberc Respir Dis. 2006;29(5):300–6.
15. Zeng Z, Lu PX, Zhou BP, et al. Imaging manifestations of human avian influenza H7N9 severe pneumonia. J Tuberc Lung Health. 2014;3(1):25–8.
16. Liang ZW, He DH, Weng WX, et al. Review and enlightenment of human avian influenza prevention and control in Hongkong. Chin J Tuberc Respir Dis. 2004;27(4):253–8.
17. Brown EG, Liu H, Kit LC, et al. Pattern of mutation in the genome of influenza A virus on adaptation to increased virulence in the mouse lung: identification of functional themes. Proc Natl Acad Sci U S A. 2001;98(12):6883–8.
18. Chen H, Deng G, Li Z, et al. The evolution of H5N1 influenza viruses in ducks in southern China. Proc Natl Acad Sci U S A. 2004;101(28):10452–7.
19. Cheung CY, Poon LL, Lau AS, et al. Induction of proinflammatory cytokines in human macrophages by influenza A (H5N1) viruses: a mechanism for the unusual severity of human disease? Lancet. 2002;60(9348):1831–7.
20. Chotpitayasunondh T, Ungchusak K, Hanshaoworakul W, et al. Human disease from influenza A (H5N1), Thailand, 2004. Emerg Infect Dis. 2005;11(2):201–9.
21. Shinya K, Hamm S, Hatta M, et al. PB2 amino acid at position 627 affects replicative efficiency, but not cell tropism, of Hong Kong H5N1 influenza A viruses in mice. Virology. 2004;320(2): 258–66.
22. Tran TH, Nguyen TL, Nguyen TD, et al. Avian influenza A (H5N1) in 10 patients in Vietnam. N Engl J Med. 2004;350(12):1179–88.
23. Carlson CM, Turpin EA, Moser LA, et al. Transforming growth factor-b: activation by neuraminidase and role in highly pathogenic H5N1 influenza pathogenesis. PLoS Pathog. 2010;6(10), e1001136.
24. Yuen KY, Wong SS. Human infection by avian influenza A H5N1. Hong Kong Med J. 2005;11(3):189–99.
25. De Jong MD, Bach VC, Phan TQ, et al. Fatal avian influenza A (H5N1) in a child presenting with diarrhea followed by coma. N Engl J Med. 2005;352(7):686–91.
26. Cai JP, Xiao R, Zhou XY. Biological characteristics and laboratory test of avian influenza virus. Chin J Lab Med. 2005;28(3):232–4.
27. Liu ST, Zhou BP, Yang DG, et al. Successful treatment of the first case of human H5N1 avian influenza in Shenzhen. Chin J Infect Dis. 2007;25(1):29–34.
28. Normile D. Avian influenza. Studies suggest why few humans catch the H5N1 virus. Science. 2006;311(5768):1692.
29. Doherty PC, Turner SJ, Webby RG, et al. Influenza and the challenge for immunology. Nat Immunol. 2006;7(5):449–55.
30. Pizza G, Amadori M, Ablashi D, et al. Cell mediated immunity to meet the avian influenza A (H5N1) challenge. Med Hypotheses. 2006;67(3):601–8.
31. Lu PX, Zhou BP, Zhu WK, et al. Imaging features of pneumonia caused by highly pathogenic H5N1 Subtype human avian influenza virus. Chin J Med ImagTechnol. 2007;23(4):532–5.
32. Lu PU, Deng YY. Epidemiological and imaging manifestations of human avian influenza. Chin Comp Med Imag. 2010;16(5):431–4.
33. Lu PX, Zhu WK, Ye RX, et al. CT manifestation and dynamic changes of grave pneumonia in adults caused by H5N1 subtype of human avian influenza virus. Chin J CT MRI. 2007;5(1):31–4.
34. Zhao DJ, Ma DQ. Imaging manifestations of human avian influenza. Chin J Radiol. 2006;40(3):319–21.
35. Puxuan L, Boping Z, et al. Radiological features of lung changes caused by avian influenza subtype A H5N 1 virus: report of two severe adult cases with regular follow -up. Chin Med J. 2010;123:100–4.
36. Tran TH, Nguyen TL, Nguyen TD, et al. Avian influenza A(H5N1) in 10 patients in Vietnam. N Engl J Med. 2004;35(12):1179–88.
37. Cheung CY, Poon LL, Lau AS, et al. Induction of proinflammatory cytokines in human macrophages by influenza A (H5N1) viruses: a mechanism for the unusual severity of human disease? Lancet. 2002;360(9348):1831–7.
38. Peiris JS, Yu WC, Leung CW, et al. Re-emergence of fatal human influenza A subtype H5N1 disease. Lancet. 2004;363(9409):617–9.
39. Lu PX, Zeng Z, Huang XR, et al. Imaging presentations and dynamic changes of severe pneumonia incurred by avian influenza H7N9. Radiol Pract. 2014;29(7):740–4.
40. Wang LQ, Shi YX, Zhang ZY, et al. Imaging preliminary observation of new recombinant avian influenza (H7N9) pneumonia. Chin J Radiol. 2013;47(6):505–8.
41. Qingle W, Zhiyong Z, Yuxin S, et al. Emerging H7N9 influenza A (Novel Reassortant Avian-Origin) pneumonia: radiologic findings [J]. Radiology. 2013;268(9):882–9.
42. Huang XH, Huang H, Lu PU, et al. CT presentations of human avian influenza H7N9 pneumonia and its correlation with viral load and CD4+ T cell. Radiol Pract. 2014;29(7):751–5.
43. Fu WJ, Hu MH, Liu XQ, et al. Retrospective analysis of one case of avian influenza H10N8 severe pneumonia in Jiangxi province. Chin J Public Health. 2014;30(6):818–9.
44. Chen HY, Yuan H, Gao RB, et al. Clinical and epidemiological characteristics of a fatal case of avian influenza A H10N8 virus infection: a descriptive study [J]. Lancet. 2014;383(9918):714–21.